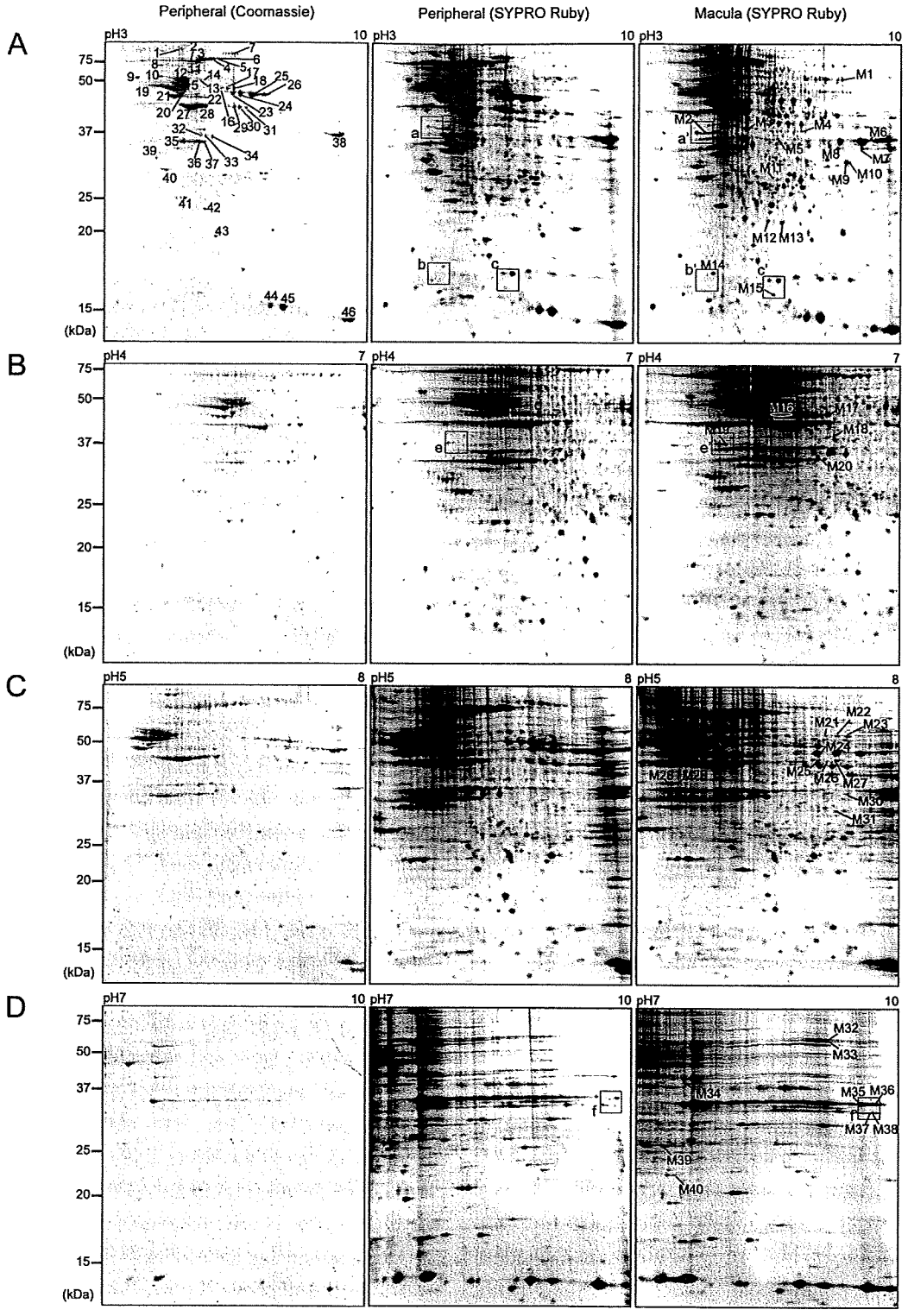

Fig. 1. Separation of monkey retina proteins on 2D gels. Proteins extracted from the peripheral retina and macula (300 μg each) were isoelectric focused at four different pH ranges; pH 3–10 (A), 4–7 (B), 5–8 (C), 7–10 (D). Then the IPG strips were separated on 12% SDS-page gels and stained by SYPRO Ruby. Forty spots marked by spot IDs were unique to the macula gel images and identified by LC-MS/MS. Boxed areas (a–f, Peripheral-SYPRO Ruby; a'–f', Macula-SYPRO Ruby) correspond to the enlarged images in Fig. 2. Two dimensional gels of peripheral retina were also stained by Bio-safe Coomassie. Forty-six spots marked by spot number were identified by LC-MS/MS.

salted prior to the IEF separation by Ready Prep 2D cleanup kit using TCA (trichloroacetic acid) acetone precipitation which resulted in successful separations. To obtain a further separation, the pH range of the 2D gel electrophoresis was narrowed to three ranges; 4–7, 5–8, and 7–10 (Fig. 1B–D). Among gel images for both the macula and peripheral retina, fluorescence from spots of abundant proteins were saturated and showed indistinct spot boundaries. Excess proteins contained in the samples were not concentrated at one spot by 2D gel electrophoresis and showed streaking and outliers. To exclude these proteins which were identified from seemingly macular specific spots, abundant proteins were identified. To clarify the outline of saturated spots, gels of peripheral retina were stained with Bio-safe Coomassie. Forty-nine proteins were identified from forty-six spots in the Coomassie stained gel image of the pH 3–10 range (Fig. 1A, Peripheral Coomassie). The proteins are listed in Table 1. Forty-eight known proteins from earlier proteomic studies of the retina were identified [1, 5, 15, 49, 50]. The neurofilament triplet L protein identified in our study has not been previously identified by the proteomic approach but it has been reported in a SAGE analysis [35]. The 49 proteins were expressed in both the macula and peripheral retina, while 26 proteins were identified from 40 spots in macula gel images (Table 2). Twenty-three of these were also reported in previous proteomic studies of the retina [1, 5, 10, 15, 22, 50]. The other three proteins are known to be ubiquitously expressed in cells [8, 11]. Therefore, these proteins were not macula specific but widely expressed in the retina.

Validation of macula enriched proteins

To obtain the relative expression levels of the identified proteins, western blot analysis was performed on the following five proteins identified by mass spectrometry: tropomyosin 1 α chain (Fig. 2A and 2E), γ-synuclein (Fig. 2B), E-FABP (Fig. 2C), arrestin-C (Fig. 2D), and hnRNPs A2/B1 (Fig. 2F). Arrestin-C has been identified as a cone photoreceptor-specific protein [33], and thus served as a positive control for this study. γ-Synuclein is a protein known to be up-regulated in cancer cells [20]. hnRNPs A2/B1 is also known to be up-regulated in carcinoma cells [42]. E-FABP is a reactive lipid scavenger [2]. Four proteins, including arrestin-C, were confirmed to have higher expression in the macula by western blotting. Tropomyosin 1 α chain has been reported to have many isoforms by alternative splicing [34]. MS/MS data from spot M2 (Fig.1A, Macula SYPRO Ruby) identified the peptide sequence CAELEEELK, which corresponded to isoform 1 (skeletal muscle type) or isoform 5 (brain type, TMBr-3) of tropomyosin 1 α chain in the UniProtKB/Swiss-Prot database. Based on these data, western blotting was performed using two antibodies for tropomyosin 1 α chain. The anti-tropomyosin antibody TM311 detects 19 amino acids in exon 1a of the tropomyosin gene family in mammalian tissues, viz., alpha-, beta-, gamma-, delta- tropomyosin, including the skeletal muscle type but it does not detect the brain type (TMBr-3), because TMBr-3 doesn't contain exon 1a in transcription sequence. The other antibodies used were specific to the brain isoforms TMBr-1 and TMBr-3 [34]. Signals of TMBr-1 were not detected in samples from the two retinal regions by western blotting (data not shown). The signals of TMBr-3 were not significantly different, and the signals to TM311 were found to be different between the two regions.

Tissue localization of macula enriched proteins

To determine the location of the 5 proteins in the macula, immunohistochemistry was performed using antibodies against each protein (Fig. 3). Arrestin-C was detected in photoreceptor outer segments and the outer plexiform layer (Fig. 3B) as previously reported [33]. γ-Synuclein was detected in RGCs in the nerve fiber layer (Fig. 3D), which confirms the result of a previous study [43]. E-FABP was predominantly detected in the outer plexiform layer and external limiting membrane, which exists between the outer nuclear layer and the photoreceptor layer (Fig. 3G). Our observation is consistent with that of an earlier study by Kingma *et al.* reporting the localization of E-FABP to Müller cells [21], which are dense in the parafovea [7]. hnRNPs A2/B1 was located in the nucleus of cells in the retinal ganglion cell layer, the inner nuclear layer, the outer nuclear layer, and the RPE with different intensities (Fig. 3E). TM311 was detected in the choroidal layer (Fig. 3F), while tropomyosin Br-3 was located in photoreceptor inner segments and the outer plexiform layer (Fig. 3C). To determine the localization of tropomyosin detected by TM311

Table 1. Proteins identified in 46 spots of Coomassie-stained gel

Spot No.[a)]	Protein name	Database accession No.[b)]	MW (kDa)[c)]	pI[c)]	Sequence coverage (%)	No. of peptide
1	Heat shock protein HSP 90-alpha	P07900	84.5	4.94	10.53	7
1	Heat shock protein HSP 90-beta	P08238	83.1	4.97	6.09	4
2	Heat shock cognate 71 kDa protein	P11142	70.9	5.37	29.41	17
2	Vacuolar ATP synthase catalytic subunit A, ubiquitous isoform	P38606	68.3	5.35	20.75	10
2	Lamin B2	Q03252	67.7	5.29	17.67	9
2	Heat shock 70 kDa protein 1	P08107	70.1	5.48	16.54	9
2	Stress-70 protein, mitochondrial	P38646	73.7	5.87	9.57	5
3	Stress-70 protein, mitochondrial	P38646	73.7	5.87	8.25	4
3	Serum albumin	P02768	69.4	5.92	6.9	4
4	Serum albumin	P02768	69.4	5.92	6.9	3
5	Serum albumin	P02768	69.4	5.92	7.39	4
6	Serum albumin	P02768	69.4	5.92	3.94	2
7	Serotransferrin	P02787	77.1	6.81	3.72	2
8	Neurofilament triplet L protein	P07196	61.4	4.64	23.99	13
9	Calreticulin	P27797	48.1	4.29	15.59	6
10	Protein disulfide-isomerase	P07237	57.1	4.76	5.12	2
11	60 kDa heat shock protein, mitochondrial	P10809	61.1	5.7	15.36	8
11	Pyruvate kinase, isozymes M1/M2	P14618	57.8	7.95	3.58	2
12	Vimentin	P08670	53.5	5.06	39.57	15
13	Vacuolar ATP synthase subunit B, brain isoform	P21281	56.5	5.57	5.09	2
14	Vacuolar ATP synthase subunit B, brain isoform	P21281	56.5	5.57	7.24	3
15	Tubulin alpha-3 chain	Q71U36	50.1	4.94	17.29	7
15	Tubulin alpha-1 chain	P68366	49.9	4.95	14.96	6
16	S-arrestin	P10523	45.1	6.14	3.7	1
17	S-arrestin	P10523	45.1	6.14	19.01	7
18	S-arrestin	P10523	45.1	6.14	22.96	8
19	Tubulin beta-2C chain	P68371	49.8	4.79	19.55	8
19	Tubulin beta-2 chain	P07437	49.7	4.78	18.92	8
19	Tubulin beta-3 chain	Q13509	50.4	4.83	16.89	7
19	Tubulin beta-6 chain	Q9BUF5	49.9	4.77	11.88	5
20	ATP synthase beta chain, mitochondrial	P06576	56.6	5.26	25.9	8
21	Gamma-enolase	P09104	47.1	4.91	12.47	5
22	Eukaryotic initiation factor 4A-II	Q14240	46.4	5.33	16.22	5
22	Eukaryotic initiation factor 4A-I	P60842	46.2	5.32	12.56	4
23	Alpha-enolase	P06733	47	6.99	31.41	9
24	Alpha-enolase	P06733	47	6.99	24.71	9
25	Alpha-enolase	P06733	47	6.99	14.32	6
26	Alpha-enolase	P06733	47	6.99	22.86	8
27	Actin, cytoplasmic 1	P60709	41.7	5.29	16.53	5
27	Actin, cytoplasmic 2	P63261	41.8	5.31	16.53	5
27	Actin, gamma-enteric smooth muscle	P63267	41.9	5.31	11.7	4
27	Actin, aortic smooth muscle	P62736	42	5.24	11.67	4
28	Creatine kinase B-type	P12277	42.6	5.34	14.17	4
29	Glutamine synthetase	P15104	41.9	6.42	6.45	3
30	Glutamine synthetase	P15104	41.9	6.42	24.73	8
31	Glutamine synthetase	P15104	41.9	6.42	6.45	2
32	L-lactate dehydrogenase B chain	P07195	36.5	5.72	7.51	2
33	L-lactate dehydrogenase B chain	P07195	36.5	5.72	27.03	7
34	L-lactate dehydrogenase B chain	P07195	36.5	5.72	39.04	11
35	Cellular retinaldehyde-binding protein	P12271	36.3	4.98	22.15	6
36	Inorganic pyrophosphatase	Q15181	32.7	5.54	11.76	3
36	Guanine nucleotide-binding protein G(I)/G(S)/G(T) beta subunit 1	P62873	37.2	5.6	6.49	2
37	Inorganic pyrophosphatase	Q15181	32.7	5.54	14.88	4
37	Guanine nucleotide-binding protein G(I)/G(S)/G(T) beta subunit 1	P62873	37.2	5.6	11.5	4
38	Malate dehydrogenase, mitochondrial	P40926	35.5	8.92	19.82	6
38	Glyceraldehyde-3-phosphate dehydrogenase	P04406	35.9	8.58	10.78	3
39	14-3-3 protein epsilon	P62258	29.2	4.63	14.51	3
40	14-3-3 protein zeta/delta	P63104	27.7	4.73	14.69	3
40	14-3-3 protein theta	P27348	27.8	4.68	14.69	3
40	14-3-3 protein gamma	P61981	28.2	4.8	13.82	3
41	Recoverin	P35243	23	5.06	10.05	2
42	ATP synthase delta chain, mitochondrial	P30049	17.5	5.38	5.36	1
43	Alpha crystallin A chain	P02489	19.9	5.77	16.76	3
44	Hemoglobin beta subunit	P68871	15.9	6.81	22.6	3
45	Hemoglobin beta subunit	P68871	15.9	6.81	22.6	3
46	Hemoglobin alpha subunit	P69905	15.1	8.73	23.4	3

[a)]Spot numbers correspond to the numbers on gel images in Fig. 1 (Peripheral-Coomassie). [b)]Accession No. corresponds to UniProtKB/Swiss-prot database. [c)]MW and pI are theoretical scores.

Table 2. Proteins identified in 40 spots detected only in macular gels

Spot No.[a)]	Protein name	Database accession No.[b)]	MW (kDa)[c)]	pI[c)]	Sequence coverage (%)	No. of peptide
M1	Pyruvate kinase, isozymes M1/M2	P14618	32.7	4.69	18.11	8
M2	Tropomyosin 1 alpha chain	P09493	32.7	4.69	13.73	5
M2	Heterogeneous nuclear ribonucleoproteins C1/C2	P07910	33.7	4.95	16.67	4
M3	Transaldolase	P37837	37.5	6.36	16.62	5
M3	3'(2'),5'-bisphosphate nucleotidase 1	O95861	33.4	5.46	10.06	3
M4	Poly(rC)-binding protein 1	Q15365	37.5	6.66	16.85	5
M5	Crk-like protein	P46109	33.8	6.26	7.59	2
M6	Heterogeneous nuclear ribonucleoproteins A2/B1	P22626	37.4	8.97	4.53	1
M7	Heterogeneous nuclear ribonucleoproteins A2/B1	P22626	37.4	8.97	11.9	3
M8	Voltage-dependent anion-selective channel protein 2	P45880	38.1	6.32	9.8	3
M9	Voltage-dependent anion-selective channel protein 1	P21796	30.6	8.63	7.8	2
M10	Voltage-dependent anion-selective channel protein 1	P21796	30.6	8.63	15.6	3
M11	Endoplasmic reticulum protein ERp29	P30040	29	6.77	27.59	6
M12	Guanylate kinase	Q16774	21.6	6.11	13.27	2
M13	Guanylate kinase	Q16774	21.6	6.11	19.39	3
M14	Gamma-synuclein	O76070	13.3	4.97	12.6	1
M15	Fatty acid-binding protein, epidermal	Q01469	15	6.8	21.64	3
M16	Arrestin-C	P36575	42.8	5.53	14.95	4
M17	Arrestin-C	P36575	42.8	5.53	4.64	1
M18	Isocitrate dehydrogenase [NAD] subunit alpha	P50213	39.6	6.46	22.4	7
M18	Transaldolase	P37837	37.5	6.36	15.73	5
M19	Tropomyosin 1 alpha chain	P09493	32.7	4.69	14.79	3
M19	Heterogeneous nuclear ribonucleoproteins C1/C2	P07910	33.7	4.95	12.75	3
M20	Pyruvate dehydrogenase E1 component beta subunit	P11177	39.2	6.2	31.75	8
M21	Glucose-6-phosphate 1-dehydrogenase	P11413	59.1	6.44	5.84	3
M22	Glucose-6-phosphate 1-dehydrogenase	P11413	59.1	6.44	9.73	5
M23	Glucose-6-phosphate 1-dehydrogenase	P11413	59.1	6.44	12.65	6
M24	26S proteasome non-ATPase regulatory subunit 11	O00231	47.3	6.09	23.04	8
M25	Elongation factor Tu	P49411	49.5	7.26	10.62	4
M26	Elongation factor Tu	P49411	49.5	7.26	4.87	2
M27	Alpha-centractin	P61163	42.6	6.19	8.78	2
M28	Heterogeneous nuclear ribonucleoproteins C1/C2	P07910	33.7	4.95	16.01	4
M29	Heterogeneous nuclear ribonucleoproteins C1/C2	P07910	33.7	4.95	22.55	6
M30	Heterogeneous nuclear ribonucleoprotein H3	P31942	36.9	6.37	11.27	3
M31	Voltage-dependent anion-selective channel protein 1	P21796	30.6	8.63	19.5	4
M31	Esterase D	P10768	31.5	6.54	4.61	1
M32	Pyruvate kinase, isozymes M1/M2	P14618	57.8	7.95	33.21	14
M33	Pyruvate kinase, isozymes M1/M2	P14618	57.8	7.95	29.43	13
M34	Aspartate aminotransferase	P17174	46.1	6.57	8.74	3
M35	Heterogeneous nuclear ribonucleoproteins A2/B1	P22626	37.4	8.97	9.92	3
M36	Heterogeneous nuclear ribonucleoproteins A2/B1	P22626	37.4	8.97	9.92	3
M37	Heterogeneous nuclear ribonucleoproteins A2/B1	P22626	37.4	8.97	7.37	2
M38	Heterogeneous nuclear ribonucleoproteins A2/B1	P22626	37.4	8.97	7.37	2
M39	Phosphoglycerate mutase 1	P18669	28.7	6.75	8.3	2
M40	Superoxide dismutase [Mn]	P04179	24.7	8.35	10.36	2

[a)]Spot ID corresponds to the numbers on gel images in Fig. 1 (Macula-SYPRO Ruby). [b)]Accession No. corresponds to UniProtKB/Swiss-prot database. [c)]MW and pI are theoretical scores.

in the choroidal layer more specifically, sections were labeled with anti-PECAM1 antibody (Fig. 3H). PECAM1 is an adhesion molecule expressed at intercellular junctions between vascular endothelial cells [24] (Fig. 3J and 3K, green). Tropomyosin detected by TM311 (red) was expressed adjacent to PECAM1 (Fig. 3I and 3K).

Discussion

In this study, we identified and validated of proteins expressed in the macula and peripheral retina. The method, 2D gel electrophoresis, limits detection to proteins in aqueous soluble form. Nevertheless, a number

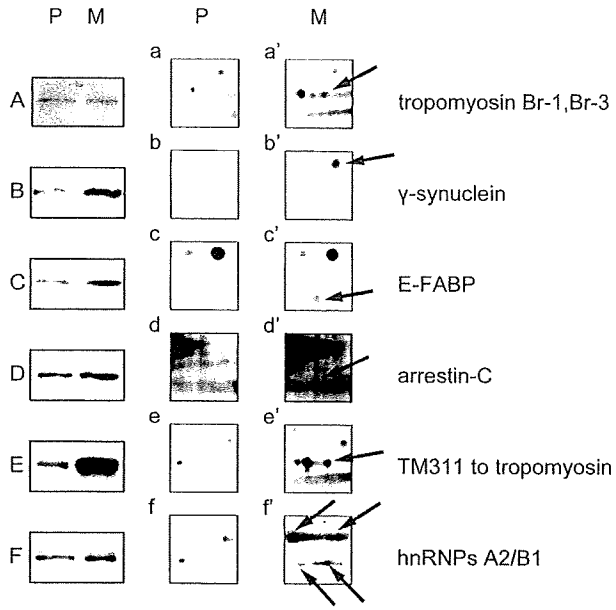

of proteins highly expressed in the macula were found.

One of the identified proteins was arrestin-C, which is known to be highly expressed in cone photoreceptors, which are densely located in the primate macula [6]. Previous SAGE analyses of the retina by Bowes Rickman *et al.* [3] have shown 1.4-fold higher transcription of arrestin-C in the macula compared to the peripheral

Fig. 2. Western blot of 5 proteins. Five micrograms of each sample from the peripheral retina and macula were loaded onto SDS-page gel (for γ-synuclein, 15 μg loading). After transferring to a PVDF membrane, the proteins were detected with antibodies specific to tropomyosin Br-1, Br-3 (A), γ-synuclein (B), E-FABP (C), arrestin-C (D), TM311 to tropomyosin (E), hnRNPs A2/B1 (F). Pieces of gel images (a–f, a'–f') correspond with the boxed areas in Fig. 1 (Peripheral-SYPRO Ruby and Macula-SYPRO Ruby). Lane P, peripheral retina; Lane M, macula.

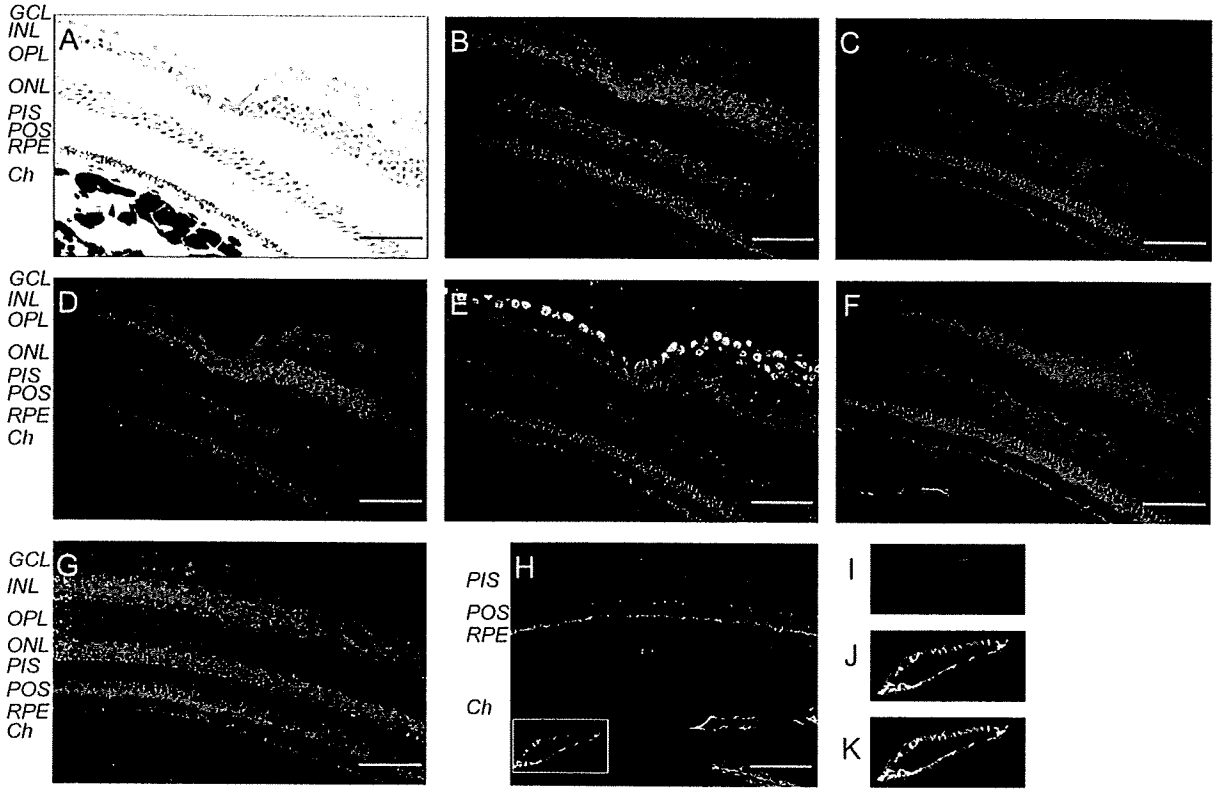

Fig. 3. Tissue localization of macula enriched proteins. Four-micrometer paraffin sections of monkey retina were stained with hematoxylin and eosin (A), other sections were labeled with antibodies specific to arrestin-C (B), tropomyosin Br-1, Br-3 (C), γ-synuclein (D), hnRNPs A2/B1 (E), TM311 to tropomyosin (F), and E-FABP (G). Tropomyosin was detected by TM311 in the choroidal layer (H). Boxed area in (H) is enlarged; labeled with antibodies specific to TM311 (red) (I), PECAM1 (green) (J), and merged (K). GCL, ganglion cell layer; INL, inner nuclear layer; OPL, outer plexiform layer; ONL, outer nuclear layer; PIS, photoreceptor inner segment; POS, photoreceptor outer segment; RPE, retinal pigment epithelial; Ch, choroid. (Bar; 50 μm)

retina in humans. Another protein that was identified in macular unique spots was 3'(2'),5'-bisphosphate nucleotidase 1 (Table 2, M3), which has also been identified by SAGE as being highly expressed in cone photoreceptors [3]. Identification of these cone photoreceptor rich proteins indicates that the present proteomic analysis was methodologically effective for identifying proteins richly expressed in the macula. It also suggests the higher protein level in the macula may be due to a higher density of specific cell types expressing specific proteins. Previous studies have shown arrestin-C expression in cones [33], γ-synuclein expression in RGCs [43], and E-FABP expression in Müller cells [21]. Although these proteins have been identified in not only specific cell types or compartments in the retina [1, 10, 15, 22, 50], the majority were localized in particular cell layers in the retina (Fig. 3B, 3D, and 3G). In a comparative transcription study of macular and peripheral RPE, expression of E-FABP was 6.3-fold higher in the peripheral RPE compared to macular RPE in middle-aged humans [48]. Our immunostaining showed predominant localization of E-FABP in the neural retina, except the photoreceptors (Fig. 3G), which is consistent with the results of Kingma *et al.* [21]. Our observation of higher E-FABP expression in the macula is due to higher expression by the neural retina, not the RPE.

Immunostaining revealed hnRNPs A2/B1 was present in every retinal nucleus layer (Fig. 3E). However, western blots showed higher expression of hnRNPs A2/B1 in the macula than in the peripheral retina (Fig. 2F). This may be explained by a higher concentration of RGC layers, where hnRNPs A2/B1 is preferentially expressed, in the macular region (Fig. 3E). hnRNPs A2/B1 was identified in several horizontal 2D gel spots (Fig. 1D, box. f') indicating the possibility of multiple phosphorylation sites for this protein. Phosphorylation of hnRNPs A2/B1 has been shown to be essential for the myelination of the axon-glia connection [51]. A similar myelination role is expected for hnRNPs A2/B1 in the RGCs.

In this study, two types of antibodies for tropomyosin isoforms were used. The brain-type isoform of tropomyosin detected by TMBr-3 antibody was not differentially expressed between the macula and peripheral retina (Fig. 2A), however tropomyosin detected by TM311 antibody showed remarkably higher expression in the macula (Fig. 2E). The difference in the expression level of the TM311-detected isoforms of tropomyosin resulted in an additional spot in the macula 2D gel which did not react with the TMBr-3 antibody. The TMBr-3-detected isoform is expressed in all regions of the brain [12, 41] and also in the outer plexiform layer and photoreceptor inner segments of the retina (Fig. 3C). This is in contrast to arrestin-C expression, which is limited to the photoreceptor outer segment (Fig. 3B). This is the first report to localize the brain-type isoform of tropomyosin in photoreceptors.

TM311 detected isoforms were localized to vascular endothelial cells compared to the localization of PECAM1 in choroid layer (Fig. 3H). Abundant expression of tropomyosin 1 α chain in the macula may arise from the higher capillary density in the choroidal layer of the fovea [30]. An earlier study, using human umbilical vein endothelial cells exposed to hydrogen peroxide, showed an increase in phosphorylation of tropomyosin through the activation of the extracellular signal-regulated kinase (ERK) pathway. Inhibition of the ERK pathway results in disruption of the endothelial layer and a two-fold increase in transendothelial permeability [17]. Tropomyosin has been previously described to interact with two anti-angiogenic factors, endostatin, a cleaved fragment of collagen XVIII [23], and high molecular weight kininogen [52]. Both proteins exhibit anti-angiogenic effect by binding to tropomyosin. Thus, tropomyosin may play an inhibitory role in increasing permeability or angiogenesis in the macula. Angiogenesis is a pathological finding often observed in the advanced stage of AMD [13].

In summary, 26 gel spots were identified as unique to the macula and 5 of these proteins were also confirmed by western blot as being richly expressed in the macula. Differential expression is likely due to morphological differences between the macula and the peripheral retina. The retina of macaque monkeys is almost identical to that of humans. Further understanding of these proteins should provide valuable information about the onset and progression of macular diseases in humans.

Acknowledgments

The authors thank Professor Duco Hamasaki for critical reading of the manuscript and helpful comments.

This study was funded in part by a grant to TI from the Ministry of Health, Labour and Welfare of Japan and by a grant to HO from the Ministry of Education, Culture, Sports, Science and Technology of Japan (KAKENHI 19791305).

References

1. Alge, C.S., Suppmann, S., Priglinger, S.G., Neubauer, A.S., May, C.A., Hauck, S., Welge-Lussen, U., Ueffing, M., and Kampik, A. 2003. Comparative proteome analysis of native differentiated and cultured dedifferentiated human RPE cells. *Invest. Ophthalmol. Vis. Sci.* 44: 3629–3641.
2. Bennaars-Eiden, A., Higgins, L., Hertzel, A.V., Kapphahn, R.J., Ferrington, D.A., and Bernlohr, D.A. 2002. Covalent modification of epithelial fatty acid-binding protein by 4-hydroxynonenal in vitro and in vivo. Evidence for a role in antioxidant biology. *J. Biol. Chem.* 277: 50693–50702.
3. Bowes Rickman, C., Ebright, J.N., Zavodni, Z.J., Yu, L., Wang, T., Daiger, S.P., Wistow, G., Boon, K., and Hauser, M.A. 2006. Defining the human macula transcriptome and candidate retinal disease genes using EyeSAGE. *Invest. Ophthalmol. Vis. Sci.* 47: 2305–2316.
4. Butt, R.H., Pfeifer, T.A., Delaney, A., Grigliatti, T.A., Tetzlaff, W.G., and Coorssen, J.R. 2007. Enabling coupled quantitative genomics and proteomics analyses from rat spinal cord samples. *Mol. Cell. Proteomics* 6: 1574–1588.
5. Cavusoglu, N., Thierse, D., Mohand-Said, S., Chalmel, F., Poch, O., Van-Dorsselaer, A., Sahel, J.A., and Leveillard, T. 2003. Differential proteomic analysis of the mouse retina: the induction of crystallin proteins by retinal degeneration in the rd1 mouse. *Mol. Cell. Proteomics* 2: 494–505.
6. Curcio, C.A., Allen, K.A., Sloan, K.R., Lerea, C.L., Hurley, J.B., Klock, I.B., and Milam, A.H. 1991. Distribution and morphology of human cone photoreceptors stained with anti-blue opsin. *J. Comp. Neurol.* 312: 610–624.
7. Distler, C. and Dreher, Z. 1996. Glia cells of the monkey retina—II. Müller cells. *Vision Res.* 36: 2381–2394.
8. Dreyfuss, G., Kim, V.N., and Kataoka, N. 2002. Messenger-RNA-binding proteins and the messages they carry. *Nat. Rev. Mol. Cell. Biol.* 3: 195–205.
9. El-Mofty, A., Gouras, P., Eisner, G., and Balazs, E.A. 1978. Macular degeneration in rhesus monkey (Macaca mulatta). *Exp. Eye Res.* 27: 499–502.
10. Ethen, C.M., Reilly, C., Feng, X., Olsen, T.W., and Ferrington, D.A. 2006. The proteome of central and peripheral retina with progression of age-related macular degeneration. *Invest. Ophthalmol. Vis. Sci.* 47: 2280–2290.
11. Feller, S.M. 2001. Crk family adaptors-signalling complex formation and biological roles. *Oncogene* 20: 6348–6371.
12. Had, L., Faivre-Sarrailh, C., Legrand, C., Mery, J., Brugidou, J., and Rabie, A. 1994. Tropomyosin isoforms in rat neurons: the different developmental profiles and distributions of TM-4 and TMBr-3 are consistent with different functions. *J. Cell Sci.* 107: 2961–2973.
13. Haddad, S., Chen, C.A., Santangelo, S.L., and Seddon, J.M. 2006. The genetics of age-related macular degeneration: a review of progress to date. *Surv. Ophthalmol.* 51: 316–363.
14. Harwerth, R.S. and Smith, E.L. 3rd. 1985. Rhesus monkey as a model for normal vision of humans. *Am. J. Optom. Physiol. Opt.* 62: 633–641.
15. Hauck, S.M., Schoeffmann, S., Deeg, C.A., Gloeckner, C.J., Swiatek-de Lange, M., and Ueffing, M. 2005. Proteomic analysis of the porcine interphotoreceptor matrix. *Proteomics* 5: 3623–3636.
16. Hope, G.M., Dawson, W.W., Engel, H.M., Ulshafer, R.J., Kessler, M.J., and Sherwood, M.B. 1992. A primate model for age related macular drusen. *Br. J. Ophthalmol.* 76: 11–16.
17. Houle, F., Rousseau, S., Morrice, N., Luc, M., Mongrain, S., Turner, C.E., Tanaka, S., Moreau, P., and Huot, J. 2003. Extracellular signal-regulated kinase mediates phosphorylation of tropomyosin-1 to promote cytoskeleton remodeling in response to oxidative stress: impact on membrane blebbing. *Mol. Biol. Cell* 14: 1418–1432.
18. Ishibashi, K., Tian, J., and Handa, J.T. 2004. Similarity of mRNA phenotypes of morphologically normal macular and peripheral retinal pigment epithelial cells in older human eyes. *Invest. Ophthalmol. Vis. Sci.* 45: 3291–3301.
19. Ishibashi, T., Sorgente, N., Patterson, R., and Ryan, S.J. 1986. Pathogenesis of drusen in the primate. *Invest. Ophthalmol. Vis. Sci.* 27: 184–193.
20. Ji, H., Liu, Y.E., Jia, T., Wang, M., Liu, J., Xiao, G., Joseph, B.K., Rosen, C., and Shi, Y.E. 1997. Identification of a breast cancer-specific gene, BCSG1, by direct differential cDNA sequencing. *Cancer Res.* 57: 759–764.
21. Kingma, P.B., Bok, D., and Ong, D.E. 1998. Bovine epidermal fatty acid-binding protein: determination of ligand specificity and cellular localization in retina and testis. *Biochemistry (Mosc)* 37: 3250–3257.
22. Liu, Q., Tan, G., Levenkova, N., Li, T., Pugh, E.N. Jr., Rux, J.J., Speicher, D.W., and Pierce, E.A. 2007. The proteome of the mouse photoreceptor sensory cilium complex. *Mol. Cell. Proteomics* 6: 1299–1317.
23. MacDonald, N.J., Shivers, W.Y., Narum, D.L., Plum, S.M., Wingard, J.N., Fuhrmann, S.R., Liang, H., Holland-Linn, J., Chen, D.H., and Sim, B.K. 2001. Endostatin binds tropomyosin. A potential modulator of the antitumor activity of endostatin. *J. Biol. Chem.* 276: 25190–25196.
24. Matsubara, T.A., Murata, T.A., Wu, G.S., Barron, E.A., and Rao, N.A. 2000. Isolation and culture of rat retinal microvessel endothelial cells using magnetic beads coated with antibodies to PECAM-1. *Curr. Eye Res.* 20: 1–7.
25. Monaco, W.A. and Wormington, C.M. 1990. The rhesus monkey as an animal model for age-related maculopathy. *Optom. Vis. Sci.* 67: 532–537.
26. Nicolas, M.G., Fujiki, K., Murayama, K., Suzuki, M.T., Mineki, R., Hayakawa, M., Yoshikawa, Y., Cho, F., and Kanai, A. 1996. Studies on the mechanism of early onset macular degeneration in cynomolgus (*Macaca fascicularis*) monkeys. I. Abnormal concentrations of two proteins in the retina. *Exp. Eye Res.* 62: 211–219.

27. Nicolas, M.G., Fujiki, K., Murayama, K., Suzuki, M.T., Shindo, N., Hotta, Y., Iwata, F., Fujimura, T., Yoshikawa, Y., Cho, F., and Kanai, A. 1996. Studies on the mechanism of early onset macular degeneration in cynomolgus monkeys. II. Suppression of metallothionein synthesis in the retina in oxidative stress. *Exp. Eye Res.* 62: 399–408.
28. Nishizawa, Y., Komori, N., Usukura, J., Jackson, K.W., Tobin, S.L., and Matsumoto, H. 1999. Initiating ocular proteomics for cataloging bovine retinal proteins: microanalytical techniques permit the identification of proteins derived from a novel photoreceptor preparation. *Exp. Eye Res.* 69: 195–212.
29. Ordya, J.M., Brizeea, K.R., and Hanscheb, J. 1980 Visual acuity and foveal cone density in the retina of the aged rhesus monkey. *Neurobiol. Aging* 1: 133–140.
30. Oyster, C.W. 1999. The Human Eye: Structure and Function, Sinauer Associates Inc., Massachusetts.
31. Provis, J.M., Penfold, P.L., Cornish, E.E., Sandercoe, T.M., and Madigan, M.C. 2005. Anatomy and development of the macula: specialisation and the vulnerability to macular degeneration. *Clin. Exp. Optom.* 88: 269–281.
32. Radeke, M.J., Peterson, K.E., Johnson, L.V., and Anderson, D.H. 2007. Disease susceptibility of the human macula: differential gene transcription in the retinal pigmented epithelium/choroid. *Exp. Eye Res.* 85: 366–380.
33. Sakuma, H., Inana, G., Murakami, A., Higashide, T., and McLaren, M.J. 1996. Immunolocalization of X-arrestin in human cone photoreceptors. *FEBS Lett.* 382: 105–110.
34. Schevzov, G., Vrhovski, B., Bryce, N.S., Elmir, S., Qiu, M.R., O'Neill, G.M., Yang, N., Verrills, N.M., Kavallaris, M., and Gunning, P.W. 2005. Tissue-specific tropomyosin isoform composition. *J. Histochem. Cytochem.* 53: 557–570.
35. Sharon, D., Blackshaw, S., Cepko, C.L., and Dryja, T.P. 2002. Profile of the genes expressed in the human peripheral retina, macula, and retinal pigment epithelium determined through serial analysis of gene expression (SAGE). *Proc. Natl. Acad. Sci. U.S.A.* 99: 315–320.
36. Snodderly, D.M., Auran, J.D., and Delori, F.C. 1984. The macular pigment. II. Spatial distribution in primate retinas. *Invest. Ophthalmol. Vis. Sci.* 25: 674–685.
37. Snodderly, D.M., Brown, P.K., Delori, F.C., and Auran, J.D. 1984. The macular pigment. I. Absorbance spectra, localization, and discrimination from other yellow pigments in primate retinas. *Invest. Ophthalmol. Vis. Sci.* 25: 660–673.
38. Snodderly, D.M., Weinhaus, R.S., and Choi, J.C. 1992. Neural-vascular relationships in central retina of macaque monkeys (*Macaca fascicularis*). *J. Neurosci.* 12: 1169–1193.
39. Stafford, T.J. 1974. Maculopathy in an elderly sub-human primate. *Mod. Probl. Ophthalmol.* 12: 214–219.
40. Stafford, T.J., Anness, S.H., and Fine, B.S. 1984. Spontaneous degenerative maculopathy in the monkey. *Ophthalmology* 91: 513–521.
41. Stamm, S., Casper, D., Lees-Miller, J.P., and Helfman, D.M. 1993. Brain-specific tropomyosins TMBr-1 and TMBr-3 have distinct patterns of expression during development and in adult brain. *Proc. Natl. Acad. Sci. U.S.A.* 90: 9857–9861.
42. Sueoka, E., Goto, Y., Sueoka, N., Kai, Y., Kozu, T., and Fujiki, H. 1999. Heterogeneous nuclear ribonucleoprotein B1 as a new marker of early detection for human lung cancers. *Cancer Res.* 59: 1404–1407.
43. Surguchov, A., McMahan, B., Masliah, E., and Surgucheva, I. 2001. Synucleins in ocular tissues. *J. Neurosci. Res.* 65: 68–77.
44. Suzuki, M.T., Terao, K., and Yoshikawa, Y. 2003. Familial early onset macular degeneration in cynomolgus monkeys (*Macaca fascicularis*). *Primates* 44: 291–294.
45. Umeda, S., Ayyagari, R., Allikmets, R., Suzuki, M.T., Karoukis, A.J., Ambasudhan, R., Zernant, J., Okamoto, H., Ono, F., Terao, K., Mizota, A., Yoshikawa, Y., Tanaka, Y., and Iwata, T. 2005. Early-onset macular degeneration with drusen in a cynomolgus monkey (*Macaca fascicularis*) pedigree: exclusion of 13 candidate genes and loci. *Invest. Ophthalmol. Vis. Sci.* 46: 683–691.
46. Umeda, S., Ayyagari, R., Suzuki, M.T., Ono, F., Iwata, F., Fujiki, K., Kanai, A., Takada, Y., Yoshikawa, Y., Tanaka, Y., and Iwata, T. 2003. Molecular cloning of ELOVL4 gene from cynomolgus monkey (*Macaca fascicularis*). *Exp. Anim.* 52: 129–135.
47. Umeda, S., Suzuki, M.T., Okamoto, H., Ono, F., Mizota, A., Terao, K., Yoshikawa, Y., Tanaka, Y., and Iwata, T. 2005. Molecular composition of drusen and possible involvement of anti-retinal autoimmunity in two different forms of macular degeneration in cynomolgus monkey (*Macaca fascicularis*). *FASEB J.* 19: 1683–1685.
48. van Soest, S.S., de Wit, G.M., Essing, A.H., ten Brink, J.B., Kamphuis, W., de Jong, P.T., and Bergen, A.A. 2007. Comparison of human retinal pigment epithelium gene expression in macula and periphery highlights potential topographic differences in Bruch's membrane. *Mol. Vis.* 13: 1608–1617.
49. Wang, Y.D., Wu, J.D., Jiang, Z.L., Wang, Y.B., Wang, X.H., Liu, C., and Tong, M.Q. 2007. Comparative proteome analysis of neural retinas from type 2 diabetic rats by two-dimensional electrophoresis. *Curr. Eye Res.* 32: 891–901.
50. West, K.A., Yan, L., Shadrach, K., Sun, J., Hasan, A., Miyagi, M., Crabb, J.S., Hollyfield, J.G., Marmorstein, A.D., and Crabb, J.W. 2003. Protein database, human retinal pigment epithelium. *Mol. Cell. Proteomics* 2: 37–49.
51. White, R., Gonsior, C., Kramer-Albers, E.M., Stohr, N., Huttelmaier, S., and Trotter, J. 2008. Activation of oligodendroglial Fyn kinase enhances translation of mRNAs transported in hnRNP A2-dependent RNA granules. *J. Cell Biol.* 181: 579–586.
52. Zhang, J.C., Donate, F., Qi, X., Ziats, N.P., Juarez, J.C., Mazar, A.P., Pang, Y.P., and McCrae, K.R. 2002. The antiangiogenic activity of cleaved high molecular weight kininogen is mediated through binding to endothelial cell tropomyosin. *Proc. Natl. Acad. Sci. U.S.A.* 99: 12224–12229.

Letter to the Editor

Stargardt Disease with Preserved Central Vision: identification of a putative novel mutation in ATP-binding cassette transporter gene

Kaoru Fujinami,[1] Masakazu Akahori,[2] Masaki Fukui,[1] Kazushige Tsunoda,[1] Takeshi Iwata,[2] and Yozo Miyake[1,3]

[1]Laboratory of Visual Physiology, National Institute of Sensory Organs, Meguro-ku, Tokyo, Japan
[2]Division of Molecular & Cellular Biology, National Institute of Sensory Organs, National Hospital Organization, Tokyo Medical Center, Meguro-ku, Tokyo, Japan
[3]Aichi Shukutoku University, Aichi, Japan, Nagakute-cho, Aichi-gun, Aichi, Japan

doi: 10.1111/j.1755-3768.2009.01848.x

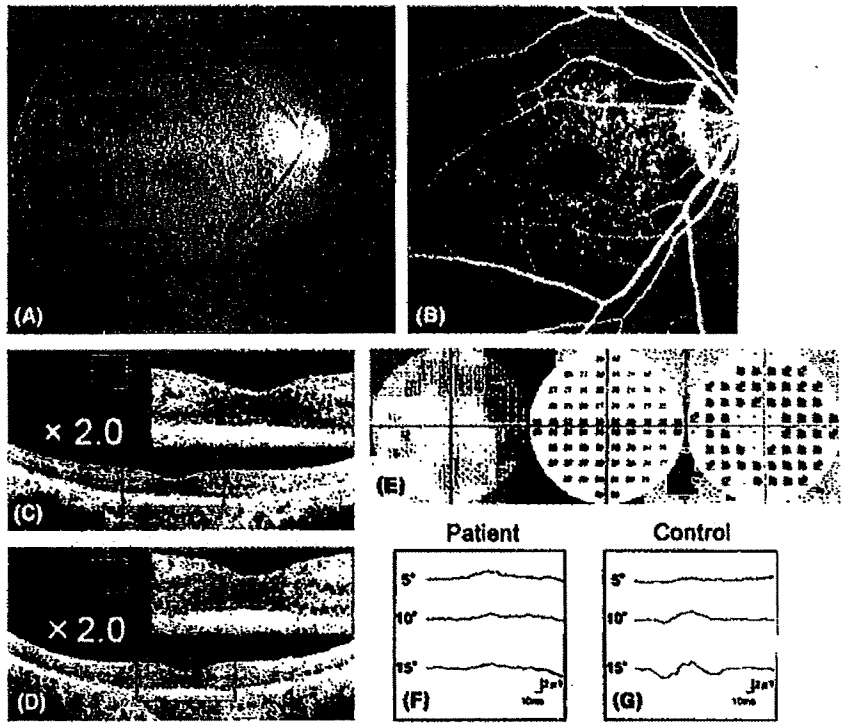

Fig. 1. Fundus photograph (A), fluorescein angiogram (FA) (B), optical coherence tomography (OCT) (C, D), Humphrey static perimetry (E), and focal macular electroretinograms (FMERGs) (F) of an eye of a patient with Stargardt disease. (A) Fundus photograph showing dark brown, well demarcated area in the fovea surrounded by orange-yellow flecks in the macula. (B) FA showing blockage in the foveal area, ring-shaped mottled hyperfluorescence in the macula, and dark choroid. (C, D) OCT images (C: horizontal, D: vertical) showing well-preserved sensory retina and retinal pigment epithelium (RPE) layer in the fovea. In the juxtafoveal region, an atrophy of both sensory retina and RPE can be seen. The enlarged images within the red lines are attached. (E) Humphrey static perimetry showing ring-shaped paracentral relative scotoma (10-2 strategy). (F, G) FMERGs showing normal responses elicited by a 5-degree stimulus spot and severely reduced responses elicited by 10-degree and 15-degree spots, when compared with the age-matched control.

Editor,

Stargardt disease (STGD) has a juvenile to young-adult onset, a rapid decrease of central vision and a progressive bilateral atrophy of the sensory retina and retinal pigment epithelium (RPE) in the macula. Yellow-orange flecks are often detected around the macula, the midretina and or both (Rotenstreich et al. 2003). Mutations in the gene encoding the ATP-binding cassette transporter gene (ABCA4) are responsible for autosomal recessive STGD (Allikmets 1997; Webster et al. 2001). We examined a patient who had the characteristic signs of STGD but had good visual acuity.

A 66-year-old man complained of photophobia and a paracentral scotoma which was present since his teens and had not worsened. None of his family members had similar symptoms. His visual acuity was 20/15 OU, and ophthalmoscopy identified a dark brown, well-demarcated area at the fovea surrounded by RPE atrophy and flecks (Fig. 1A). Fluorescein angiography showed window defects at the flecks and a dark choroid (Fig. 1B). The optical coherence tomographic (OCT) images showed a well-preserved sensory retina and normal thickness RPE at the fovea (Fig. 1C, D). The foveal area was surrounded by atrophic sensory retina and RPE. Static perimetry showed ring-shaped paracentral relative scotoma which surrounded the normal area seeing area of 5° (Fig. 1E). Focal macular electroretinograms (FMERGs) also demonstrated a well-preserved retinal function at the fovea (Fig. 1F). Compared to age-matched controls, the FMERGs had normal responses elicited by a 5-degree stimulus spot and severely reduced responses elicited by 10-degree and 15-degree spots (Fig. 1F, G). Genetic analysis with direct DNA sequencing of amplified products revealed four reported polymorphisms (Allikmets 1997; Briggs et al. 2001; Webster et al. 2001; Fukui et al. 2002) and one novel mutation, Met280Thr, in exon 7 of the ABCA4 gene (Table 1).

Our patient had clinical findings that were pathognomonic of typical STGD, except that the clinical course was stationary and he had 20/15 vision because of well-preserved foveal function. The preserved foveal area was small and well demarcated. Visual acuity, fundus appearance, OCT images, static perimetry and FMERGs supported the well-preserved foveal function. We report our case because the patient had a unique phenotype with a novel putative mutation in the *ABCA4* gene, not yet shown to segregate with the disease.

The well-demarcated dark brown foveal RPE appeared to be hyperpigmented although the thickness measured by OCT was 29 μm which was

Table 1. ABCA4 GENE MUTATION AND Polymorphisms.

Exon	Nucleotide Change	Effect Changes	Het/Hom	References
Mutation				
7	c.839T > C	p.Met280Thr	Het	Present study
Polymorphisms				
10	c.1269C > T	p.His424His	Hom	Webster AR et al.
45	c.6249C > T	p.Ile2083Ile	Het	Allikmets R et al.
46	c.6285T > C	p.Asp2095Asp	Het	Briggs CE et al.
49	c.6764G > T	p.Ser2255Ile	Het	Allikmets R et al.

The translational start codon ATG/methionine is numbered as +1. One novel disease-associated mutation [c.839T > C (p.Met280Thr)] was found. References of previously reported polymorphisms are indicated.
Het, heterozygote; Hom, homozygote.

within normal limits. The findings in our case could indicate that the non-atrophic foveal RPE had an effect in preserving the foveal morphology and function.

The inheritance of STGD is autosomal recessive; however, our patient had four polymorphisms and one heterozygous gene mutation c.839T > C in exon 7 in the *ABCA4* gene. A second mutation was not found, but it may well exist outside of the coding sequence of the *ABCA4* gene. The new mutation in our patient was located outside the known functional domains of ATP-binding or transmembrane site (Lewis et al. 1999), which may explain the mild effect of the missense mutation. We should also consider a modifier gene effect in our patient.

Although the relationship between the new mutation of the *ABCA4* gene and the well-preserved foveal structure is unresolved, the unique phenotype and genotype of our patient may give additional information on the mechanism of photoreceptor degeneration in eyes with STGD.

References

Allikmets R (1997): A photoreceptor cell-specific ATP-binding transporter gene (ABCR) is mutated in recessive Stargardt macular dystrophy. Nat Genet 17: 122.

Briggs CE, Rucinski D, Rosenfeld PJ, Hirose T, Berson EL & Dryja TP (2001): Mutations in ABCR (ABCA4) in patients with Stargardt macular degeneration or cone-rod degeneration. Invest Ophthalmol Vis Sci 42: 2229–2236.

Fukui T, Yamamoto S, Nakano K et al. (2002): ABCA4 gene mutations in Japanese patients with Stargardt disease and retinitis pigmentosa. Invest Ophthalmol Vis Sci 43: 2819–2824.

Lewis RA, Shroyer NF, Singh N et al. (1999): Genotype/Phenotype analysis of a photoreceptor-specific ATP-binding cassette transporter gene, ABCR, in Stargardt disease. Am J Hum Genet 64: 422–434.

Rotenstreich Y, Fishman GA & Anderson RJ (2003): Visual acuity loss and clinical observations in a large series of patients with Stargardt disease. Ophthalmology 110: 1151–1158.

Webster AR, Heon E, Lotery AJ et al. (2001): An analysis of allelic variation in the ABCA4 gene. Invest Ophthalmol Vis Sci 42: 1179–1189.

Correspondence:
Kazushige Tsunoda, MD
Laboratory of Visual Physiology
National Institute of Sensory Organs
2-5-1 Higashigaoka
Meguro-ku
Tokyo 152-8902
Japan
Tel: + 81 3 3411 0111 ext. 6615
Fax: + 81 3 3412 9811
Email: tsunodakazushige@kankakuki.go.jp

OPEN ACCESS Freely available online

PLoS one

VAV2 and *VAV3* as Candidate Disease Genes for Spontaneous Glaucoma in Mice and Humans

Keiko Fujikawa[1,3,6]*, Takeshi Iwata[2], Kaoru Inoue[3], Masakazu Akahori[2], Hanako Kadotani[1], Masahiro Fukaya[4], Masahiko Watanabe[4], Qing Chang[5], Edward M. Barnett[5], Wojciech Swat[6]

1 Department of Pathology and Immunology, Hokkaido University Graduate School of Medicine, Sapporo, Japan, **2** National Institute of Sensory Organs, National Hospital Organization Tokyo Medical Center, Tokyo, Japan, **3** Faculty of Health Science, Hokkaido University, Sapporo, Japan, **4** Department of Anatomy, Hokkaido University Graduate School of Medicine, Sapporo, Japan, **5** Department of Ophthalmology and Visual Sciences, Washington University School of Medicine, St. Louis, Missouri, United States of America, **6** Department of Pathology and Immunology, Washington University School of Medicine, St. Louis, Missouri, United States of America

Abstract

Background: Glaucoma is a leading cause of blindness worldwide. Nonetheless, the mechanism of its pathogenesis has not been well-elucidated, particularly at the molecular level, because of insufficient availability of experimental genetic animal models.

Methodology/Principal Findings: Here we demonstrate that deficiency of Vav2 and Vav3, guanine nucleotides exchange factors for Rho guanosine triphosphatases, leads to an ocular phenotype similar to human glaucoma. Vav2/Vav3-deficient mice, and to a lesser degree Vav2-deficient mice, show early onset of iridocorneal angle changes and elevated intraocular pressure, with subsequent selective loss of retinal ganglion cells and optic nerve head cupping, which are the hallmarks of glaucoma. The expression of Vav2 and Vav3 tissues was demonstrated in the iridocorneal angle and retina in both mouse and human eyes. In addition, a genome-wide association study screening glaucoma susceptibility loci using single nucleotide polymorphisms analysis identified *VAV2* and *VAV3* as candidates for associated genes in Japanese open-angle glaucoma patients.

Conclusions/Significance: Vav2/Vav3-deficient mice should serve not only as a useful murine model of spontaneous glaucoma, but may also provide a valuable tool in understanding of the pathogenesis of glaucoma in humans, particularly the determinants of altered aqueous outflow and subsequent elevated intraocular pressure.

Citation: Fujikawa K, Iwata T, Inoue K, Akahori M, Kadotani H, et al. (2010) *VAV2* and *VAV3* as Candidate Disease Genes for Spontaneous Glaucoma in Mice and Humans. PLoS ONE 5(2): e9050. doi:10.1371/journal.pone.0009050

Editor: Patrick Callaerts, Katholieke Universiteit Leuven, Belgium

Received January 22, 2009; **Accepted** January 18, 2010; **Published** February 4, 2010

Funding: The work described in this report was funded in parts by a grant from the Ministry of Education, Culture, Sports, Science and Technology in Japan. The funders had no role in study design, data collection and analysis, decision to publish, or preparation of the manuscript.

Competing Interests: The authors have declared that no competing interests exist.

* E-mail: fujikawa@med.hokudai.ac.jp

Introduction

The critical importance of elevated intraocular pressure (IOP) in the pathogenesis of glaucomatous optic neuropathy is widely recognized [1,2]. While compromise of aqueous humor outflow is the key determinant of elevation in IOP [3,4], the molecular mechanisms underlying changes in the outflow pathway that lead to elevated IOP remain to be elucidated. For this reason, mouse genetic knockout models of spontaneous glaucoma are highly sought after.

The Vav proteins are the best-characterized family of guanine nucleotide exchange factors (GEFs) that activates Rho guanosine triphosphatases (GTPases) in a phosphorylation-dependent manner [5]. Rho GTPases control cell behavior via regulating the specific filamentous actin structures involved in migration, adhesion, and morphogenesis, by acting as binary switches cycling between an inactive (GDP-bound) and active (GTP-bound) state [6]. The three mammalian Vav proteins, Vav1, Vav2, and Vav3, share a Dbl homology domain for their enzymatic activity as GEFs and contain a common structural array characteristic of proteins involved in signal transduction. Regardless of the structural similarity, Vav proteins differ in their tissue distribution. Vav1 is expressed specifically in lymphoid lineage cells, whereas Vav2 and Vav3 are more widely expressed [5,7]. Genetic approaches using knockout mice have provided valuable information on the function of Vav proteins *in vivo*. Vav proteins are crucial for the development and function of hematopoietic lineage cells such as lymphocytes, neutrophils, natural killer cells, and osteoclasts [8–16]. Individual Vav proteins exhibit both redundant and specialized functions. Despite the wide distribution of Vav2 and Vav3 proteins in mouse tissues, little is known about their specific function in non-hematopoietic cells.

While trying to better elucidate the functions of Vav2 and Vav3 in non-hematopoietic cells, we discovered that Vav2/Vav3-deficient mice have a significant ocular phenotype. Specifically, we show that Vav2/Vav3-deficient mice have elevated IOP, which eventually manifests as buphthalmos. Loss of Vav2 and Vav3 expression is associated with changes in the iridocorneal angle, with eventual chronic angle closure. The elevation of IOP in Vav2/Vav3-deficient mice is accompanied by an optic

neuropathy characterized by selective loss of retinal ganglion cells (RGCs) and optic nerve head (ONH) excavation and is therefore consistent with glaucoma. In addition, both *VAV2* and *VAV3* are shown to be susceptibility loci by single nucleotide polymorphisms (SNPs) study of Japanese primary open-angle glaucoma patients.

Results

Vav2/Vav3-Deficient Mice Develop Buphthalmos

Eyes of Vav2/Vav3-deficient ($Vav2^{-/-}Vav3^{-/-}$) mice were noted to develop buphthalmos starting between 6 and 12 weeks of age (Figure 1). This enlargement was typically seen unilaterally at first, with frequent bilateral involvement over the next 1–2 months, and continued enlargement until the mice were 6-months old. Eventually, some of the eyes, became atrophic and phthisical in appearance (Figure 1A). In order to confirm our initial observations, we measured the corneal diameters and weights of $Vav2^{-/-}Vav3^{-/-}$ mice eyes and compared them with age-matched wild-type mice eyes (Figure 1B). The examination clearly showed our observations were relevant. We observed 200 $Vav2^{-/-}Vav3^{-/-}$ mice at 6 months of age and almost 75% of them showed the enlarged eyes (Figure 1C). In addition, histological study indicated that there were no abnormal findings in the tissues both around the enlarged eyes such as inflammation, tumor, or hyperplasia, and in the thyroid of the $Vav2^{-/-}Vav3^{-/-}$ mice (data not shown).

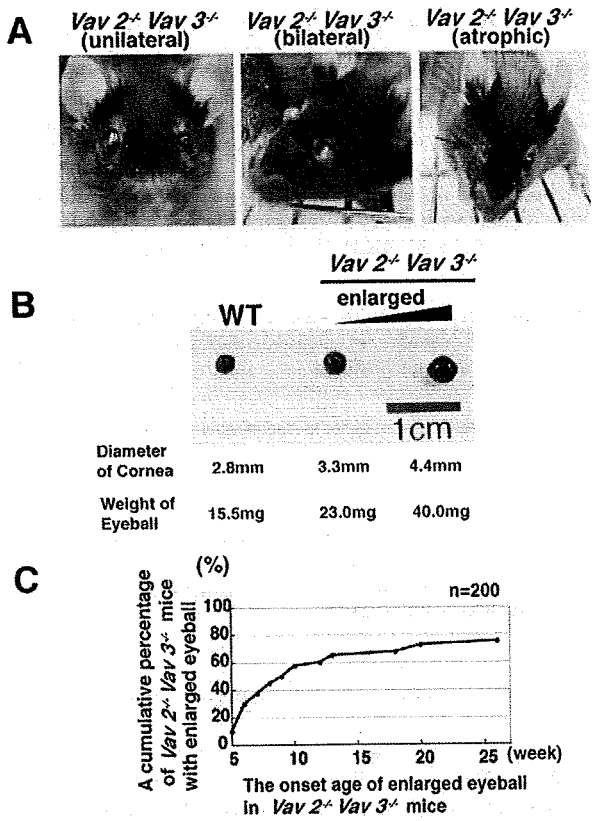

Figure 1. Vav2/Vav3-deficient mice develop buphthalmos. Eyes of Vav2/Vav3-deficient ($Vav2^{-/-}Vav3^{-/-}$) mice develop buphthalmos between 6 and 12 weeks of age. **A.** Left photo: Representative photo of unilateral enlarged eye in 10-week-old $Vav2^{-/-}Vav3^{-/-}$ mice. Centre photo: Representative photo of bilateral enlarged eyes in 16-week-old $Vav2^{-/-}Vav3^{-/-}$ mice. Right photo: Representative photo of enlarged eye becoming atrophic in 8-week-old $Vav2^{-/-}Vav3^{-/-}$ mice. **B.** Comparison of eye sizes. Left panel: Representative eye of 10-week-old wild-type (WT) mice as a control (n = 20). Cornea diameter is 2.9±0.1 mm. Weight is 15.8±1.1 mg. Centre panel: Representative first-recognized enlarged eye of $Vav2^{-/-}Vav3^{-/-}$ mice (9- to 10-week-old, n = 20). The cornea diameter is 3.3±0.1 mm. Weight is 23.7±4.4 mg. $P<0.001$. Right panel: Representative moderately enlarged eye of 12-week-old $Vav2^{-/-}Vav3^{-/-}$mice (n = 20). The cornea diameter is 4.2±0.4 mm. Weight is 38.0±4.0 mg. **C.** Age of onset of enlarged eyes up to 25 weeks of age in $Vav2^{-/-}Vav3^{-/-}$ mice (n = 200). The vertical axis is a cumulative percentage of $Vav2^{-/-}Vav3^{-/-}$ mice with enlargement of the eyes.
doi:10.1371/journal.pone.0009050.g001

Elevation of Intraocular Pressure of Vav-Deficient Mice

As we observed the development of buphthalmos, we assessed for elevated IOP in $Vav2^{-/-}Vav3^{-/-}$, Vav2-deficient ($Vav2^{-/-}$), and Vav3-deficient ($Vav3^{-/-}$) mice. IOP was measured using a rodent tonometer (Tonolab) starting at 4 weeks post-natal and were compared with age-matched wild-type C57BL/6 mice. Reliable measurement of IOP before 4 weeks of age was not possible. At 6 weeks of age, $Vav2^{-/-}Vav3^{-/-}$ mice first showed increased IOP (18.2±3.1 vs. 14.0±2.4 mmHg, $p<0.05$), with further increases out to 10 weeks of age (22.5±7.4 vs. 14.6±4.2 mmHg, $p<0.01$) (Figure 2A). IOP measurements in $Vav2^{-/-}Vav3^{-/-}$ mice ranged from 11–40 mmHg between 7 weeks and 16 weeks of age. There was a statistically significant difference in IOP between the $Vav2^{-/-}Vav3^{-/-}$ and wild-type mice at all time points demonstrated. The phenotype of littermate wild type mice was identical to that of the "inbred" C57BL/6 strain (Figure S1).

In $Vav2^{-/-}$ mice, elevated IOP was first detected at 7 weeks of age. The IOP for $Vav2^{-/-}$ mice was found to be increased at 8 weeks of age compared to wild-type mice (15.5±3.7 vs. 14.0±4.2 mmHg, $p<0.05$)(Figure 2B). The IOP of $Vav2^{-/-}$ mice showed further increases at 10 weeks of age (18.1±3.7 vs. 14.6±4.2 mmHg, $p<0.01$) and remained significantly higher at 12 weeks. In contrast, the IOP of $Vav3^{-/-}$ mice did not differ significantly from wild-type mice between 8 and 12 weeks (Figure 2C). The phenotype of littermate wild type mice was identical to that of inbred strain "C57BL/6". We also demonstrated that the phenotype of Vav2 and Vav3 heterozygous littermate mice ($Vav2^{+/-}$, and $Vav3^{+/-}$) were same as that of wild type (Figure S1).

Retinal Ganglion Cell Loss and Optic Nerve Head Changes in Vav2/Vav3-Deficient Mice

We next examined whether Vav2/Vav3-deficient ($Vav2^{-/-}Vav3^{-/-}$) mice showed changes in the retinal ganglion cell (RGC) layer and optic nerve head (ONH). At 3 weeks of age, $Vav2^{-/-}Vav3^{-/-}$ mice did not show any histological difference in the ONH or the number of RGCs compared to that of age-matched wild-type mice (Figure 3A). At 10 weeks of age, following several weeks of IOP elevation, early signs of ONH cupping and cell body loss in the RGC layer were apparent in $Vav2^{-/-}Vav3^{-/-}$ mice (Figure 3B). At 15 and 30 weeks of age, $Vav2^{-/-}Vav3^{-/-}$ mice showed further evidence of ONH cupping and RGC loss in the context of an otherwise normal retinal architecture. These findings are consistent with a selective loss of RGCs with corresponding changes in the ONH, which are the hallmarks of glaucoma.

Iridocorneal Angle Histopathology in Vav-Deficient Mice

As histopathological examination of globes from mice with buphthalmos frequently demonstrated angle closure, we compared

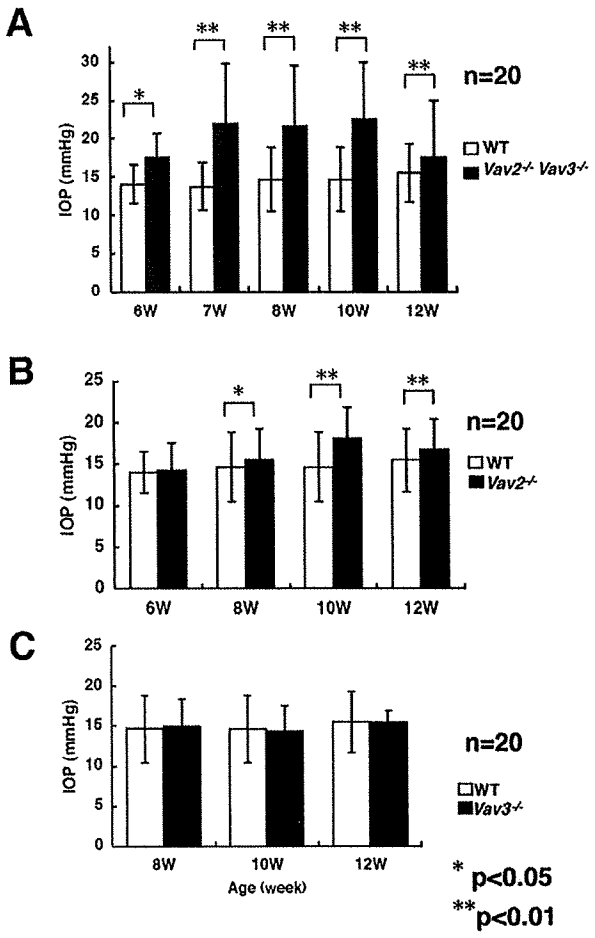

Figure 2. Elevated intraocular pressure of $Vav2^{-/-}Vav3^{-/-}$ and $Vav2^{-/-}$ mice. The intraocular pressure (IOP) of Vav2/Vav3-deficient ($Vav2^{-/-}Vav3^{-/-}$), Vav2-deficient ($Vav2^{-/-}$), and Vav3-deficient ($Vav3^{-/-}$) mice were measured between 10–12 AM. At the indicated ages, twenty mice were examined, respectively. For the IOP measurement of each Vav-deficient mouse, IOP of an age-matched wild-type (WT) mouse was also measured under the same conditions. We confirmed that these results were reproducible with four independent examinations. **A.** IOPs of $Vav2^{-/-}Vav3^{-/-}$ mice were dramatically elevated at 6 weeks of age. **B.** $Vav2^{-/-}$ mice also showed elevated IOP from around 8 weeks of age. **C.** $Vav3^{-/-}$ mice have normal range of IOP at any age. Error bars represent S.D. *P<0.05, **P<0.01 versus WT mice.
doi:10.1371/journal.pone.0009050.g002

the iridocorneal angle histology of 20 Vav2/Vav3-deficient ($Vav2^{-/-}Vav3^{-/-}$) mice with wild-type mice at both 7 and 12 weeks of age. Angles were classified as either being completely open, displaying evidence of partial occlusion of the trabecular meshwork (TM) as manifest by peripheral anterior synechiae (PAS), or being completely closed (total occlusion of the trabecular meshwork)(Figure 4A). Over half of the Vav2/Vav3-deficient mice already showed evidence of angle closure by 7 weeks of age, increasing to nearly 80% in 12-week-old mice (Figure 4B).

We also examined the correlation between elevated IOP and angle changes in 7-week-old $Vav2^{-/-}Vav3^{-/-}$ mice respectively (n = 20) (Figure S2). The mean and standard deviation of IOP in 7-week-old wild-type mice (n = 18) were 13.7±3.12 mmHg respectively. The 95th percentile of those IOPs using a normal curve was 18.8 mmHg. So that IOP over 18.8 mmHg was regarded as elevated IOP. $Vav2^{-/-}Vav3^{-/-}$ mice with elevated IOP showed evidence of angle closure by histological analysis, while $Vav2^{-/-}Vav3^{-/-}$ mice with non-elevated IOP displayed either open angles or evidence of early angle closure (PAS) and angle closure.

In addition, to characterize the progression of angle changes, two additional time points were added to this analysis of the iridocorneal angle −18 days and 4 weeks of age (n = 20 each). While at 18 days of age nearly half of the eyes demonstrated open angles, a large percentage already showed evidence of PAS (Figure 4B). By 4 weeks of age, $Vav2^{-/-}Vav3^{-/-}$ mice showed increasing frequencies of both PAS and angle closure. Taken as a whole, the data showed a gradual progression from open angles to PAS formation to closed angle from 18 days to 12 weeks.

The iridocorneal angles of Vav2-deficient ($Vav2^{-/-}$) and Vav3-deficient ($Vav3^{-/-}$) mice were examined histologically and graded in a similar manner. The iridocorneal angles of $Vav2^{-/-}$ mice also demonstrated evidence of progressive angle closure, but to a lesser extent as compared with $Vav2^{-/-}Vav3^{-/-}$ mice (Figure 4B). $Vav3^{-/-}$ mice had normal appearing open angles without evidence of PAS formation or angle closure (Figure 4B).

In order to better investigate the status of iridocorneal angles in $Vav2^{-/-}Vav3^{-/-}$ mice, we stained for myocilin as a marker for TM cells, as myocilin is strongly expressed in TM cells [17]. We examined 7-week-old $Vav2^{-/-}Vav3^{-/-}$ mice with non-elevated IOP who had either open angles or who displayed evidence of angle closure. As shown in Figure S3, myocilin was not detected in the iridocorneal angle of $Vav2^{-/-}Vav3^{-/-}$ mice with angle closure, but was seen in mice with open angles similar to those of wild-type mice.

Effects of Ocular Hypotensives in Vav2/Vav3 -Deficient Mice

We next tested the efficacy of ocular hypotensives used for human glaucoma in $Vav2^{-/-}Vav3^{-/-}$ mice with elevated IOP (Figure S4). The elevated IOP of 7-week-old $Vav2^{-/-}Vav3^{-/-}$ mice was dramatically reduced by ocular hypotensives used in humans, such as latanoprost, a prostaglandin analogue (Figure S4A). We also tested the IOP-lowering effect in $Vav2^{-/-}Vav3^{-/-}$ mice by two other ocular hypotensives, dorzolamide and timolol, whose mechanisms of action differ from that of latanoprost [18–20], being aqueous suppressants (Figure S4B). Furthermore, we tested Y-27632, a Rho-associated protein kinase inhibitor, that has been reported to cause a reduction in IOP presumably by altering cellular behavior of TM cells [21–23]. Y-27632 showed no effect of lowering IOPs against $Vav2^{-/-}Vav3^{-/-}$ mice, while it lowered the IOP significantly in age-matched wild-type mice (Figure S4C).

Expression of Vav2 and Vav3 in Mouse and Human Eyes

In order to understand the pathogenesis of the Vav2/Vav3-deficient eye phenotype, we examined the mRNA and protein expression patterns of Vav2 and Vav3 in the eye (Figure 5). Quantitative real-time PCR revealed that Vav2 and Vav3 mRNA are expressed in TM, cornea, retina, lens, iris, and ciliary body in the mouse eye (Figure 5A). Vav3 mRNA was more abundantly expressed than that of Vav2 in the TM and the retina. Gene expression levels of both Vav2 and Vav3 in the eye were comparable to levels found in immune cells where Vavs play a critical role [5,7–16]. Next, the Vav2 and Vav3 mRNA localization in mouse eye was examined by in situ hybridization (ISH) analysis (Figure 5B). Both Vav2 and Vav3 oligo probes (antisense), we used here, have been examined the specificities before and proved to have its specificity. As negative controls for

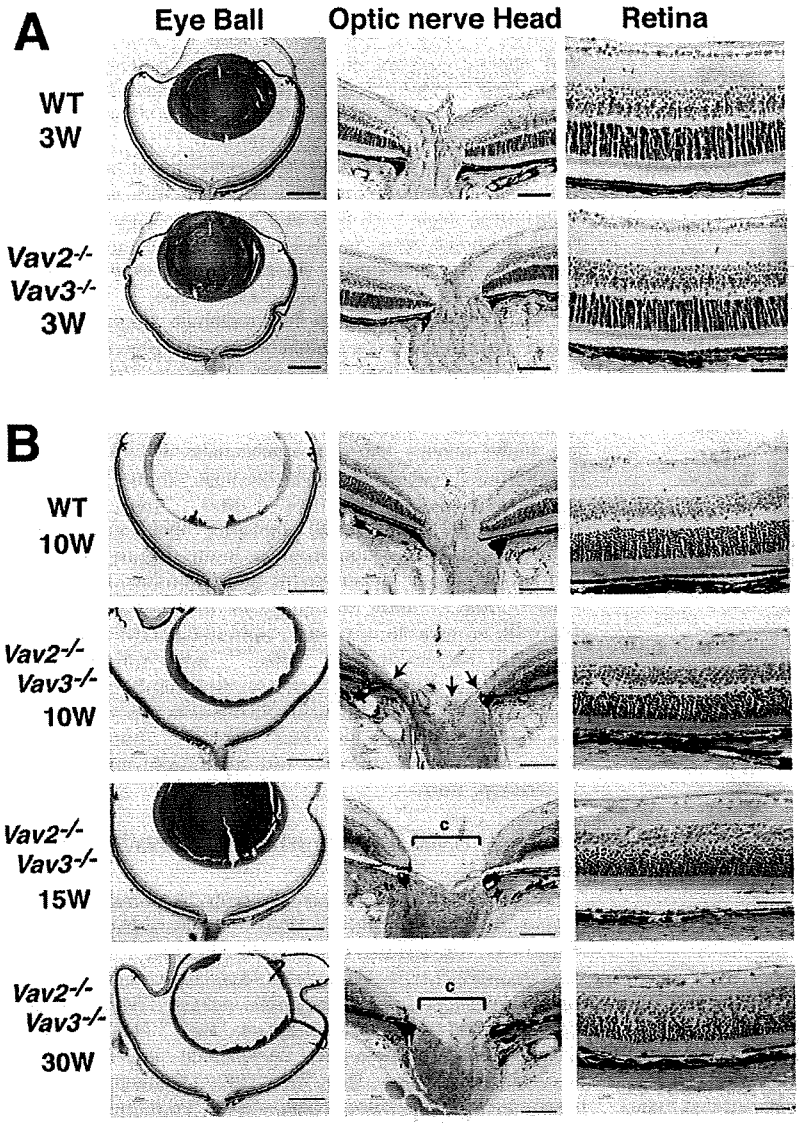

Figure 3. Optic nerve head degeneration and decrease in RGCs observed in *Vav2*$^{-/-}$*Vav3*$^{-/-}$ mice with elevated IOP. Light-microscopic histological examination is conducted to evaluate retinal neuropathy in Vav2/Vav3-deficient (*Vav2*$^{-/-}$*Vav3*$^{-/-}$) mice. **A.** At the age of 3 weeks, *Vav2*$^{-/-}$ *Vav3*$^{-/-}$ mice exhibited impairment of angle status, but no abnormal findings of Optic nerve head degeneration (ONH) or retinal ganglion cells (RGCs) in the retinas. Scale bars, from left to right side: 500 μm, 100 μm, and 50 μm. **B.** After elevation of IOP, compared to control wild-type (WT) mice in the upper panel, ONH in 10-, 15-, and 30-week-old *Vav2*$^{-/-}$*Vav3*$^{-/-}$ mice present so-called capping (shown in c) and thin retinal neural layers (indicated by arrows in the photos). In those retinas, RGCs are decreased. Scale bars, from left to right side: 500 μm, 100 μm, and 50 μm. Sections are representative from 6–12 samples.
doi:10.1371/journal.pone.0009050.g003

these experiments, we used sense probes of Vav2 and Vav3, respectively, which showed no detectable signal (Figure S5). Both genes expression were widely distributed in the ocular tissues including the iridocorneal angle, retina, cornea, and sclera. The co- localization of Vav2 and Vav3 mRNA expression in iridocorneal angle, such as TM, was confirmed by ISH. Also, we assessed Vav2 and Vav3 protein expression by immunoblotting in both mouse and human eyes (Figure 5C). In mouse eyes, expression of both Vav2 and Vav3 was demonstrated in several ocular tissues including the iridocorneal angle, retina, cornea, and sclera. Both Vav2 and Vav3 proteins were also expressed in human retina and iridocorneal angle. The migrated bands were absent in the liver extracts of the *Vav2*$^{-/-}$*Vav3*$^{-/-}$ mice. Results of densitometric ratio (Vav3/Vav2) from normalized protein loading in each lane revealed that Vav3 was more abundantly expressed than Vav2 in the iridocorneal angle tissues of both mouse and human eyes and also in the retina.

Single Nucleotide Polymorphisms in Japanese Primary Open-Angle Glaucoma Patients

We observed Vav2 and Vav3 proteins expression in the tissues of human iridocorneal angle and retina. In order to investigate the

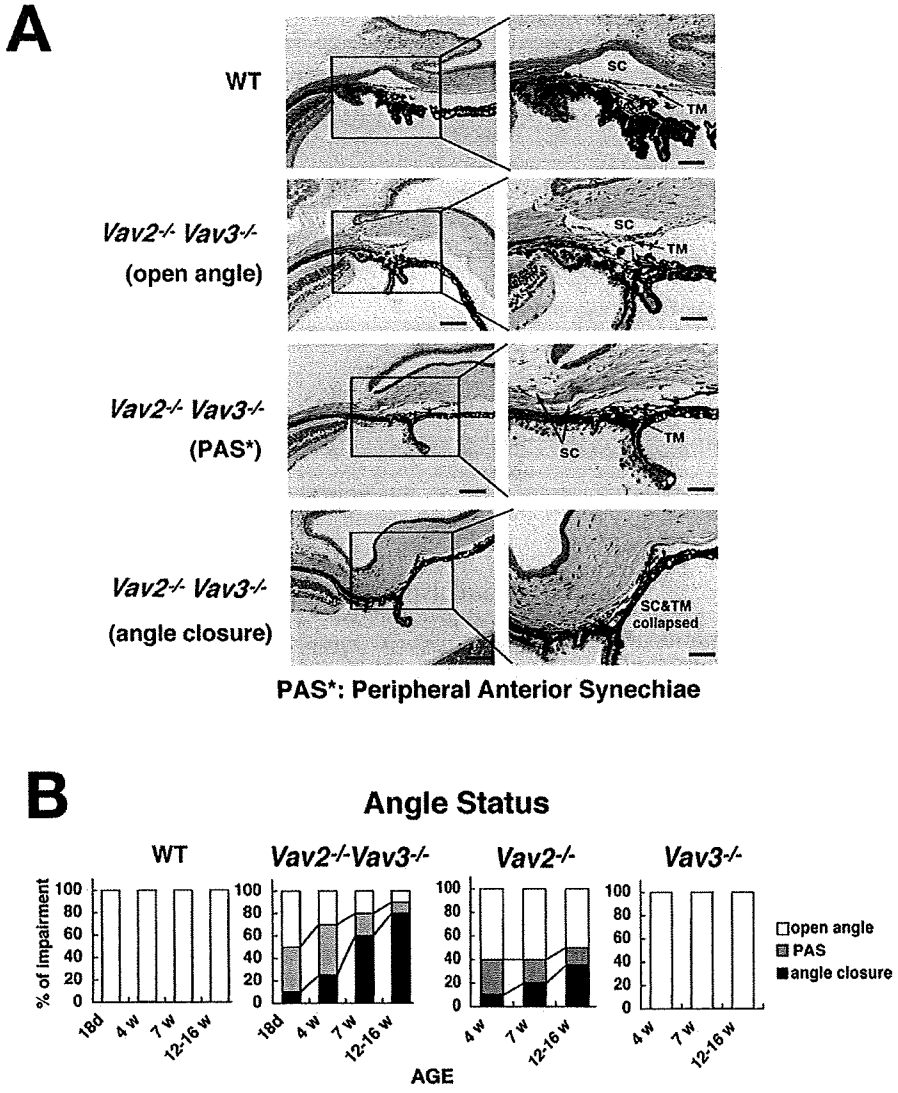

Figure 4. Characterization of progressive iridocorneal angle closures in $Vav2^{-/-}Vav3^{-/-}$ and $Vav2^{-/-}$ mice. The aqueous humor outflow facility, trabecular meshwork (TM) and Schlemm's canal (SC) (iridocornial angle) in Vav2/Vav3-deficient ($Vav2^{-/-}Vav3^{-/-}$) mice are evaluated in histological manner. Vav2-deficient ($Vav2^{-/-}$) mice also have the same changes, but of lower severity. **A.** Representative photos of normal TM and SC histology of 12-week-old wild-type (WT) mice as a control. Representative photos of normal open angle, peripheral anterior synechiae (PAS) in 12-week-old $Vav2^{-/-}Vav3^{-/-}$ mice, and angle closure status in 12-week-old $Vav2^{-/-}Vav3^{-/-}$ mice. Sections used here are all representative from 20 samples. Scale bars: left photos, 200 μm; right photos, 100 μm. **B.** Changes of angle status appear at the early ages. We classify angle status of $Vav2^{-/-}Vav3^{-/-}$, $Vav2^{-/-}$, and $Vav3^{-/-}$mice into open angle, PAS, and angle closure by histological evaluation. We find the changes of angle status at the early ages, such as in 18-day-old $Vav2^{-/-}Vav3^{-/-}$ *mice* (n = 20) and in 4-week-old of $Vav2^{-/-}Vav3^{-/-}$ *mice* (n = 20). We took four ($Vav2^{-/-}Vav3^{-/-}$) and three ($Vav2^{-/-}$, $Vav3^{-/-}$) different age groups, with 20 mice examined, respectively.
doi:10.1371/journal.pone.0009050.g004

relevant association of *VAV2* and *VAV3* in human glaucoma patients, we carried out a genome-wide association study using the Affymetrix GeneChip Human Mapping 500 K Array Set. We examined Japanese primary open–angle glaucoma (POAG) cases and age-matched non-glaucoma controls. Both *VAV2* and *VAV3* loci in Japanese POAG patients showed SNPs against the non-glaucoma controls for dbSNPs rs2156323 and rs2801219, respectively. We reported the most extreme (Table 1). Both were intronic SNPs, SNP rs2156323 lying in intron3 of *VAV2* and SNP rs2801219 lying in intron1 of *VAV3*. *VAV2* SNP rs2156323 in particular indicated significant association with Japanese POAG, including a 5.65 heterozygote odds ratio (95% confidence interval (CI): 1.99–16.0), 4.34 heterozygote relative risk (95% CI: 1.72–10.44) and 4.38×10^{-4} genotypic *P* value with respect to risk allele A.

Judging from alleric *P*-values distribution for detecting *VAV2* ranking and genotypic *P*- values distribution for *VAV3* ranking, we observed that *VAV2* and *VAV3* showed high scores ($-\log_{10}(P)$) among approximately 380,000 SNPs analyzed in this study (Figure 6). On the contrary, *VAV1* showed no association with the POAG. These data strongly suggest that *VAV2* and *VAV3* genes are susceptibility loci in Japanese POAG.

Table 1. Vav2, Vav3, Vav1 association study for POAG using the Affymetrix GeneChip.

Gene	*VAV2*	*VAV3*	*VAV1*
SNP ID	rs2156323	rs2801219	rs2617815
Chromosome Location	9q34.1	1p13.3	19p13.2
Position	133750375	108214454	6746147
Genotypic *P* value	4.38×10^{-4}	5.42×10^{-4}	4.41×10^{-2}
Allele	AG	AC	AG
Risk allele	A	C	G
Minor allele	A	C	G
Heterozygote odds ratio (95%CI)	5.65 (1.99–16.0)	2.03 (1.01–4.09)	1.04 (0.52–2.08)
Heterozygote relative risk (95%CI)	4.34 (1.72–10.44)	1.31 (1.00–1.75)	1.01 (0.82–1.23)
Homozygote odds ratio	Not Available	Not Available	Not Available
Exon Intron	*VAV2* Intron3	*VAV3* Intron1	*VAV1* Intron1
SNP type	iSNP*1	iSNP	iSNP

*1: intronic S.

doi:10.1371/journal.pone.0009050.t001

Discussion

To our knowledge, this is the first report of a spontaneous glaucoma phenotype in Vav2 ($Vav2^{-/-}$) or Vav2/Vav3-deficient ($Vav2^{-/-}Vav3^{-/-}$) mice. Vav2/Vav3-deficiency is associated with progressive iridocorneal angle changes and elevation of IOP in mice. Subsequent selective loss of RGCs and progressive ONH cupping are associated with this elevated IOP, as has previously been demonstrated in other rodent models of glaucoma [24]. The finding that Vav2-deficiency alone results in a glaucoma phenotype suggests that the absence of Vav2 plays a critical role in the development of this phenotype. Despite our finding that Vav3-deficiency did not result in either iridocorneal angle changes or elevated IOP, the more severe glaucomatous phenotype demonstrated in $Vav2^{-/-}Vav3^{-/-}$ mice as compared with $Vav2^{-/-}$ mice is consistent with an additive effect.

A number of induced glaucoma models have been established in rats and mice [24]. Each model has advantages and disadvantages, related to factors such as the ease of inducing elevated IOP, the magnitude, duration and variability of elevated IOP, and secondary effects on the eye. Due to the ease of genetic manipulation, mouse models are becoming increasingly popular over those in rats. Despite the lack of a lamina cribosa as found in human eyes, the mouse is a good genetic model to study the pathogenesis of human glaucoma as aqueous physiology and anterior segment anatomy are similar to that found in humans [25].

Other spontaneous models of glaucoma have been described in mice, most notably in DBA/2J mice. The pigmentary glaucoma phenotype demonstrated in the DBA/2J mice has been extensively studied at genetic, clinical, morphological and pathological levels [26–29]. A limitation of this model is that the elevated IOP phenotype is not primary but secondary due to the systemic pigment dispersion syndrome with the associated mutations in the *Gpnmb* and *Tyrp1* loci [26–30]. In these mice, recessive mutations in these 2 genes are associated with iris degeneration characterized by iris stromal atrophy and pigment dispersion with subsequent reduced outflow facility secondary to pigment and cell debris. Therefore, it is difficult to tie-in the identified mutations to the pathogenesis of any primary form of human glaucoma.

The Vav2/Vav3-deficient mouse has several characteristics which make it particularly useful as an animal glaucoma model. The elevated IOP occurs spontaneously in these genetically manipulated mice and does not require the ocular manipulation necessary in induced models. The frequency of the ocular phenotype is high and onset occurs at a relatively young age. In addition, ocular hypotensives commonly used to treat human glaucoma show efficacy in lowering IOP in this model. The most significant advantage of this mouse glaucoma model is that the deleted genes, Vav2 and Vav3, are well-focused targets that have been studied over 20 years providing a useful starting point for further investigation of the potential molecular mechanisms underlying this phenotype.

Several aspects of this model of spontaneous glaucoma will require further study and clarification, although we speculated from our histological results and the correlation between elevated IOP and angle status changes that anatomic angle closure is the possible mechanism for elevated IOP in this model. While progressive angle closure may be the etiology prior to elevated IOP in mice lacking Vav2 and Vav3 function, it may alternatively be a subsequent change related to other alterations in angle structures which might also affect aqueous humor outflow. In addition, since the expression of Vav2 and Vav3 was detected in ocular tissues other than those comprising the iridocorneal angle, it will be necessary in future studies to consider how their deficiency in these tissues might have potentially contributed to the spontaneous glaucoma phenotype in any way.

While so far there are several reports of glaucoma associated candidate genes based on the single nucleotide polymorphisms (SNPs) study in the Japanese population [31–36], our data first suggest that *VAV2* and *VAV3* are susceptibility loci in Japanese primary open–angle glaucoma (POAG) cases. In addition, so far we could not find the report of non-Japanese glaucoma association case study that demonstrated *VAV2* and/or *VAV3* as candidate gene loci for glaucoma [37–43]. They demonstrated glaucoma associated candidate genes study with SNPs analysis focusing on the other specific target genes, although we are interested in the *VAV2* and/or *VAV3* glaucoma association study using the different populations. This work would be important investigation to be done.

Although our current findings do not address the molecular mechanisms underlying glaucoma phenotypes, it is interesting to consider possible mechanisms based on what is currently known about Vav protein function. The TM has been regarded as a key determinant of IOP and has been implicated as the major site of

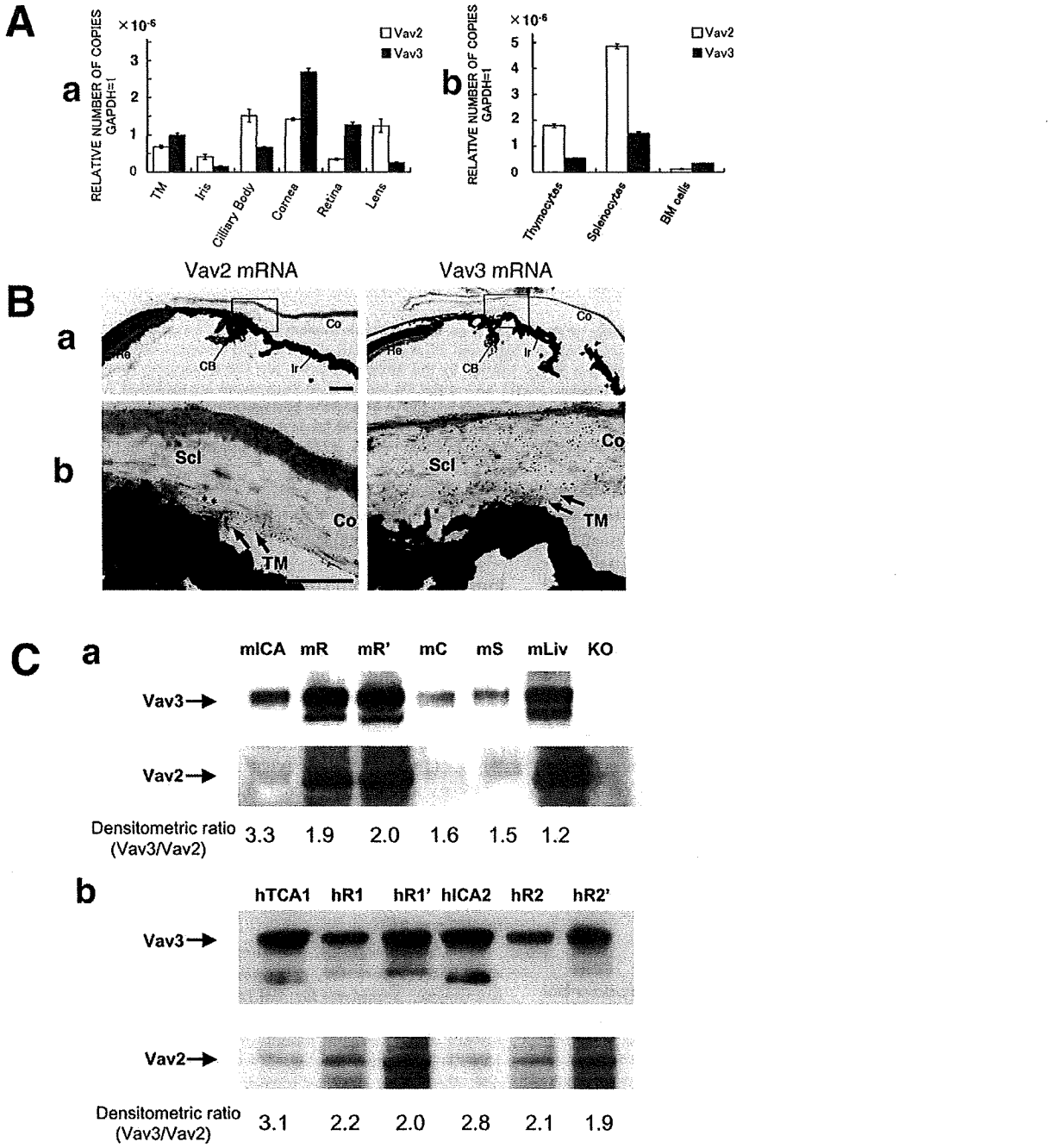

Figure 5. Vav2 and Vav3 expression in mouse and human eyes. A. Quantitative real time PCR analysis is performed for Vav2 and Vav3 mRNA expression study. The vertical axis is the copy number of Vav2 or Vav3 mRNA when that of mGAPDH is taken as 1. The assay method is absolute quantification (standard curve). **a.** Both Vav2 and Vav3 mRNA are expressed in all tissues of the murine eyes including the trabecular meshwork (TM), cornea, sclera, and retina. **b.** Vav2 and Vav3 mRNA expression level of murine immune cells. The levels of Vav2 and Vav3 expression in eye tissues are the same as those of the immune cells where Vav2 and Vav3 play the critical role. **B. a.** In situ hybridization analysis of emulsion-dipped sections display the distribution of Vav2 and Vav3 mRNA in the anterior chamber. The localization of Vav2 and Vav3 mRNA in trabecular meshwork(TM), ciliary body (CB), cornia(CO), iris(Ir), sclera (Scl) and retina(Re) by in situ hybridization. **b.** Vav2 and Vav3 mRNA expression are both detected in iridocorneal angle, such as TM (indicated by arrows in the photos). Scale bars, 50 μm. **C.** Expression of Vav2 and Vav3 proteins in mouse (**a**) and human (**b**) eyes. Vav2 and Vav3 proteins were detected in mouse or human ocular extracts (from two independent postmortem eye globe samples; at death age of 58 (1) and 87 (2)) by western blotting. Densitometric ratios (Vav3/Vav2) were shown under the blotting panels. mICA: mouse iridocorneal angle tissues, mR: mouse retina, mR': 3-fold increased loading mouse retina, mC: mouse cornea, mS: mouse sclera, mLiv: normal mouse liver(positive control), KO: Vav2/Vav3-deficient mouse as a negative control, hICA: human iridocorneal angle tissue,hR1: human retina 1, hR1': human retina1' (3-fold loading). doi:10.1371/journal.pone.0009050.g005

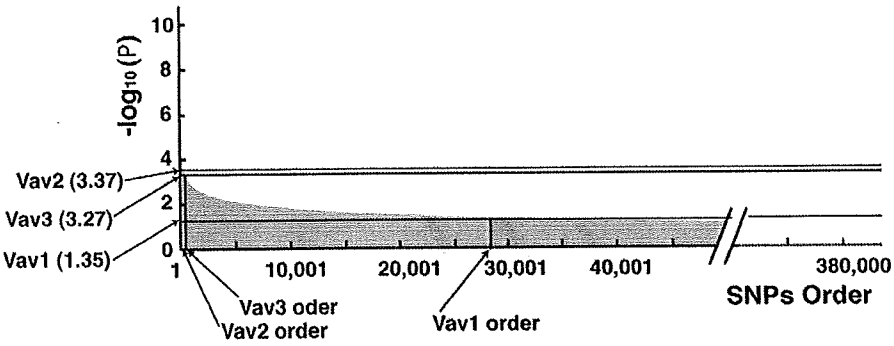

Figure 6. *VAV2* and *VAV3* genome-wide SNPs high ranking of *P*-value scores. Genome-wide ranking orders of *P*-value indicate that *VAV2* and *VAV3* are strongly susceptible genes with Japanese POAG cases. Clinically diagnosed Japanese POAG 100 cases and non-glaucoma age-matched 100 controls are examined for this study. The analysed SNPs number is about 380,000 by the Affymetrix GeneChip 500 K Mapping Array Set. The SNPs data under the 85% call rate, under 0.001 Hardy-Weinberg equilibrium (HWE), and under 5% minor allele frequencies are excluded. Allelic frequency $\chi 2$ test and genotypic frequency $\chi 2$ test are calculated respectively. The vertical axis is $-\log 10$ (*P*) and the horizontal axis is SNPs order which showed high scores from left to right. The Upper graph is alleric *P*-values distribution of *VAV2* analysis and the lower graph is genotypic *P*-values for *VAV3* and *VAV1* study. *VAV2* is located at high position in rank and *VAV3* also located at high position in rank. *VAV1* shows no association for POAG cases here.
doi:10.1371/journal.pone.0009050.g006

increased resistance to aqueous outflow which occurs in human glaucoma [44,45]. Recent findings indicate that signals emanating from integrins, key regulators of the actin cytoskeleton in trabecular meshwork cells, may be involved in control of outflow facility and Rho GTPases would be important downstream effectors of integrin-mediated actin cytoskeletal dynamics [4,46–48]. Considering the Vavs function as GEF, dysregulation of Rho is one possible mechanism by which pathology in the iridocorneal angle might result and is one that deserves further study.

In summary, we had demonstrated that Vav2/Vav3-deicient mice develop a spontaneous glaucoma phenotype. In addition, our data first suggest that *VAV2* and *VAV3* are susceptibility loci in Japanese primary open-angle glaucoma (POAG) cases. We believe that Vav2/Vav3-deficient mice will serve not only as a useful murine model of spontaneous glaucoma, but may also provide a valuable tool in understanding of the pathogenesis of glaucoma in humans, particularly the determinants of altered aqueous outflow and elevated IOP.

Materials and Methods

Mice

Vav3$^{-/-}$, *Vav2*$^{-/-}$ and *Vav2*$^{-/-}$*Vav3*$^{-/-}$ mice were described previously [15]. Mice were backcrossed at least 9 times with C57BL/6 mice (Clea Japan, Tokyo, Japan) to have the C57BL/6 background. All mice used in these experiments were bred and maintained in the SPF Facility of Hokkaido University Graduate School of Medicine in a 12-hour light-dark cycle. All mice experiments were approved by the Animal Ethics Committee of Hokkaido University Graduate School of Medicine and were conducted in accordance with the ARVO Statement for the Use of Animals in Ophthalmic and Vision Research.

Tissue Preparation and Histology

Eyes were quickly enucleated from each age group of knock-out mice and C57BL/6 wild-type control mice after deep anesthesia with pentobarbital sodium solution, then immediately fixed with solution of 2.5% glutaraldehyde (TAAB, EM Grade) in 10% formalin neutral buffer-methanol solution deodorized for anterior chamber study, or fixed with Davidson' solution for retinal analysis for 12 hours. Following this, the eyes were embedded in paraffin and dissected sagittally using a microtome into 5 μm sections. After deparaffinization and rehydration, the sections were stained with hematoxylin and eosin (Sigma).

Immunohistochemistry

The eyes were sectioned at 5 μm thickness along the vertical meridian through the optic nerve head. After deparaffinization and rehydration, the tissue sections were incubated with blocking solution containing 1% BSA in PBS for 1 hour. This was followed by 1 hour incubation with rabbit polyclonal antibody to myocilin at 1:200 in blocking solution as first antibody for 1 hour at room temperature. Anti-rabbit IgG conjugated with Alexa 488 (Molecular Probes, Eugene, OR) at 1:400 in PBS containing 0.1% Tween 20 was used as secondary antibody for 1 hour at room temperature. The stained tissues were examined using confocal fluorescence laser microscope (Radius 2000, Bio-Rad, Hercules, CA). For negative control of the immunohistochemical staining, the sections were incubated with blocking solution without primary antibody (data not shown).

Real Time PCR

Each tissue was freshly taken from SPF level C57BL/6 mice and immediately used for generating RNA by TRIzol reagent (Invitrogen). Templates for real time PCR were made by Cloned AMV Reverse Transcriptase (Invitrogen). Probes of mVav2 and mVav3 were TaqMan probes (Vav2: Mm00437287_m1, Vav3: Mm00445082_m1) purchased from Applied Biosystems (Foster city, CA). The standard curves were constructed by mVav2, mVav3 inserted plasmids, normalized by mGAPDH (Product Code: 4352339E, Applied Biosystems). All the PCR studies were performed by Applied Biosystems 7500 Real Time PCR System following the manufacturer's recommended procedures. The assay method was absolute quantification (standard curve).

In Situ Hybridization

The detailed procedure was described as previously [49]. Briefly, to detect mRNAs for Vav2 and Vav3, specific antisense oligonucleotide probes were synthesizedas follows:(2275–2319;45mers)5′-AGCTG-GAGACCGGCTTGAGGCC CTGCTGGTGGTTCGCTCCCG-AGA-3′ for Vav2 mRNA (GenBank accession No. NM_009500) and (2346–2302;45mers)5′–GTTGCCTGTTCTATTACCCCTCTG T CCAGCTGGCTGTTCTGGCTC-3′ for Vav3 mRNA (accession No. NM_020505). Oligonucleotide probes were labeled with [33P]

dATP using terminal deoxyribonucleotidyl transferase (Invitrogen, Carlsbad, CA). Under deep pentobarbital anesthesia, the eyeballs were freshly obtained from Adult C57BL/6J mice. Fresh frozen sections (20 μm thickness) were cut with a cryostat (CM1900, Leica, Nussloch,Germany) and mounted on glass slides precoated with 3-aminopropyltriethoxysilane. Sections were exposed to Nuclear Track emulsion (NTB-2, Kodak) for 5 weeks. Emulsion-dipped sections were stained with methyl green pyronine solution. The specificity of the hybridizing signals was verified by the disappearance of signals when hybridization was carried out with sense probes.

Western Blotting

Mouse Ocular Tissue Dissection: 8-week male C57BL/6J mice (Jackson Laboratory, ME) were used for ocular tissue samples. The animals were euthanized by carbon dioxide inhalation in an induction chamber. The globes were promptly enucleated after euthanization and washed in ice-cold PBS. Ocular tissues were microscopically dissected. Dissection of Postmortem Human Eye Globes: Human eyes without previous eye diseases including glaucoma were acquired from a local eye bank (Heartland Lions Eye Banks; Columbia, MO) within 6 hours post-mortem. Dissected mouse and postmortem human ocular tissues were lysed in a tissue extraction buffer (BioChain, CA). The concentration of protein supernatants was determined by a protein assay kit (Bio-Rad, CA). Rabbit polyclonal anti-mouse Vav2 (1:1000) (Santa Cruz Biotechnology, CA), monoclonal anti-human Vav2 (1:2000) (Cell Signaling Technology, MA), polyclonal anti-mouse and anti-human Vav3 (1:3000 for each) (Millipore, CA) antibodies were used for detection.

Intraocular Pressure (IOP) Measurement

IOP was measured using the TonoLab rebound tonometer for rodents (Tiolat i-care, Finland) according to the manufacturer's recommended procedures. All IOP measurements were performed between 10 AM and noon in conscious condition. Mice were gently restrained first by hand and placed on a soft towel bed on the desk and usually appeared calm and comfortable. These data were confirmed to be reproducible by three additional different independent studies (n = 20).

Evaluation of Eye Drop Medications for High Intra-Ocular Pressure of Vav2Vav3-Deficient Mice

Vav2$^{-/-}$*Vav3*$^{-/-}$ mice were housed in SPF barrier facility in standard lighting conditions (12-hour light-dark cycle). The 7–9 week after birth mice were used for the experiment. Four independent experiments were carried out to confirm the results reproducible.

Preparation and Application of Ophthalmic Solution

Latanoprost was purchased from Cayman Chemical Co. (Ann Arbor, MI) and dissolved in its vehicle solution (0.02% benzalkonium chloride, 0.5% monosodium phosphate monohydrate, 0.6% disodium hydrogen phosphate dihydrate and 0.4% sodium chloride). With a micropipette, 3 μl of PG analogue (latanoprost; prostaglandin F2α) solution or vehicle was randomly applied to the eyes of *Vav2*$^{-/-}$*Vav3*$^{-/-}$ mice. Before administration, IOP was measured with the tonometer from 10–12 AM and then the PG analogue 0.005% 3 μl or vehicle solution was applied in a masked manner. Evaluation of IOP-lowering effect was performed by measuring the IOP with the tonometer at 3 hours after drug instillation also in a masked manner. Furthermore, two different mechanistic medications, 3 μl of timolol maleate (0.5%, Merck, Whitehouse Station, NJ) or 3 μl of dorzolamide hydrochloride (1%, Trusopt; Merck), was also tested, respectively, after measuring the IOP under the same conditions as those of the Latanoprost application. Evaluation of IOP-lowering effects was performed by measuring the IOP with tonometer at 2 hours after drug instillation under blinded test protocols. Y-27632 was purchased from Carbiochem (La Jolla, CA) and dissolved in its vehicle solution (phosphate buffered saline). Y-27632 (1 mM) or vehicle solution was administered to the central cornea as a 3 μl drop by pipetting in a masked manner. Evaluation of IOP-lowering effect was performed by measuring the IOP with the tonometer at 1 hour after drug instillation.

Statistical Analysis of IOPs

Data are reported as means ± S.D. Two-tailed Student's t-test was used to compare between two groups of results. Differences between any two groups were regarded as significant when $P<0.01$(**) or $P<0.05$ (*).

Disease Associated Genome-Wide Analysis

One hundred clinically-diagnosed cases (male 46; female 54) with primary open-angle glaucoma over 30 years of age (mean age, 71.60 years; SD, 9.33 years) and non-glaucoma age-matched controls (mean age, 66.71 years; SD, 12.00 years) in a Japanese population were examined for this study. Informed consent was obtained from all participants, and the procedures used conformed to the tenets of the Declaration of Helsinki. Genomic DNAs were isolated from the peripheral blood of the POAG cases and age-matched controls for genotyping analysis. Genotyping was performed using the Affymetrix GeneChip Human Mapping 500 K Array Set (Affymetrix Services Laboratory, California). We omitted the SNP data under an 85% call rate, under 0.001 Hardy-Weinberg equilibrium (HWE), and under 5% minor allele frequency. Data analysis was performed using the LaboServer System (World Fusion, Tokyo Japan). An allelic frequency χ^2 test and genotypic frequency χ^2 test were calculated, respectively with respect to risk allele. The Odds ratio was calculated in three manners such as per allele odds ratio, heterozygote odds ratio, and homozygote odds ratio. Relative risk was also calculated, the same as for the odds ratio. The most significant SNPs were chosen in this report to evaluate the association of *VAV2*, *VAV3*, and *VAV1* in the cases.

Supporting Information

Figure S1 The comparison of intraocular pressures in age matched wild-type inbred C57BL/6 mice, wild-type littermate controls, and Vav2 and Vav3 heterozygous mice (Vav2$^{+/-}$, and Vav3$^{+/-}$). Intraocular pressures (IOPs) were measured using the TonoLab rebound tonometer for rodents from 6-week to 12-week, as described in the Methods. The phenotype of littermate wild-type mice was identical to that of the "inbred" C57BL/6 strain. The phenotype of Vav2 and Vav3 heterozygous mice were similar to that of wild-type. n = 20.
Found at: doi:10.1371/journal.pone.0009050.s001 (0.45 MB TIF)

Figure S2 The correlation between elevated IOP and angle changes in Vav2/Vav3-deficient mice. The IOP was measured in 7-week-old Vav2/Vav3-deficient (Vav2$^{-/-}$Vav3$^{-/-}$) mice (n = 20), followed by examination of the angle status by histology. While Vav2$^{-/-}$Vav3$^{-/-}$ mice with elevated IOP displayed histological evidence of angle closure, mice without elevated IOP showed either normal open angles or evidence of angle changes, angle closure or peripheral anterior synechiae. The mean and standard deviation of IOP in wild-type mice at 7-week-old (n = 18) were 13.7±3.12 mmHg, respectively. The 95th percentile of those

IOPs using a normal curve was 18.8 mmHg. IOP over 18.8 mmHg was regarded here as elevated IOP.
Found at: doi:10.1371/journal.pone.0009050.s002 (0.57 MB TIF)

Figure S3 Anti-myocilin staining of trabecular meshwork in Vav2/Vav3-deficient mice. Immunohistochemical staining of trabecular meshwork with anti-myocilin antibody in representative iridocorneal angle sections of age-matched wild-type and Vav2/Vav3-deficient ($Vav2^{-/-}Vav3^{-/-}$) 7-week-old mice with normal IOP, with either evidence of angle closure, or normal open angles similar to wild type mice. Myocilin (green-labeled), which is strongly expressed in TM cells, was regarded as a marker for TM cells. In $Vav2^{-/-}Vav3^{-/-}$ mice with angle closure, myocilin was not detected in the iridocorneal angle (indicated by arrows). Conversely, it was detected in sections from mice with normal open angles, similar to those in wild type mice. Blue fluorescence is DAPI counter staining. Scale bars, 20 um.
Found at: doi:10.1371/journal.pone.0009050.s003 (2.19 MB TIF)

Figure S4 Effects of ocular hypotensives in Vav2/Vav3-deficient mice. A. Ocular hypotensives used for human glaucoma, latanoprost, a prostaglandin analogue was tested in 7-week-old Vav2/Vav3-deficient ($Vav2^{-/-}Vav3^{-/-}$) mice with elevated IOP ($n = 20$). The IOP was measured 3 hours before and after topical application of 3 μl of 0.01% latanoprost in a masked manner. Vehicle was used as a control. Latanoprost lowered the IOP significantly in $Vav2^{-/-}Vav3^{-/-}$ mice (26.3 ± 5.0 mmHg versus 15.8 ± 5.1 mmHg; $n = 20$), while the IOP was not altered by the vehicle alone. The latanoprost-induced reduction of IOP in $Vav2^{-/-}Vav3^{-/-}$mice was statistically significant (**$P<0.01$, $n = 20$). The data shown are representative of three independent experiments performed. Error bars represent S.D. **$P<0.01$ versus vehicle-treated $Vav2^{-/-}Vav3^{-/-}$ mice. B. Using three different drugs for lowering IOP, we compared the effects by percentages of elevated IOP reduction. These data are representative from three independent experiments, respectively ($n = 20$). Error bars represent S.D. **$P<0.01$ versus vehicle-treated $Vav2^{-/-}Vav3^{-/-}$ mice. C. Rho-associated protein kinase Inhibitor, Y-27632 was tested for lowering IOP on $Vav2^{-/-}Vav3^{-/-}$ mice ($n = 20$). Y27632 administration has no effect against $Vav2^{-/-}Vav3^{-/-}$ mice (before, 19.69 ± 4.98 mmHg; after, 18.83 ± 5.60 mmHg; $n = 20$), while Y-27632 lowered the IOP significantly in age-matched wild-type mice (13.58 ± 2.27 mmHg versus 12.31 ± 1.94 mmHg; $n = 20$. $p<0.05$) and the IOP was not altered by the vehicle solution (13.25 ± 1.71 mmHg versus 13.18 ± 3.17 mmHg; $n = 20$). These data are representative from four independent experiments, respectively. Error bars represent S.D. *$P<0.05$ versus vehicle-treated WT mice.
Found at: doi:10.1371/journal.pone.0009050.s004 (0.41 MB TIF)

Figure S5 Sense probe staining for in situ hybridization experiments in ocular tissues. In situ hybridization with Vav2 and Vav3 sense probes were carried out as negative controls for the experiments. C57BL/6 mouse ocular tissue sections including the iridocorneal angle, sclera and cornea were used. With sense probes, there was no detectable signal around mouse iridocorneal angle tissues. TM; trabecular meshwork. Scl; sclera.
Found at: doi:10.1371/journal.pone.0009050.s005 (4.14 MB TIF)

Acknowledgments

The authors thank Professor Duco Hamasaki (Bascom Palmer Eye Institute, University of Miami School of Medicine, Florida) and Morton Smith, M.D. (Washington University Department of Ophthalmology & Visual Sciences) for helpful suggestions and discussion; and Mr. Tsutomu Osanai and Ms. Takae Oyama for technical help.

Author Contributions

Conceived and designed the experiments: KF TI KI. Performed the experiments: KF TI MA HK MF QC. Analyzed the data: KF TI KI MA MF MW EMB WAS. Contributed reagents/materials/analysis tools: KF TI KI MW WAS. Wrote the paper: KF KI EMB WAS.

References

1. Kass MA, Heuer DK, Higginbotham EJ, Johnson CA, Keltner JL, et al. (2002) The ocular hypertension treatment study: a randomized trial determines that topical ocular hypotensive medication delays or prevents the onset of primary open-angle glaucoma. Arch Ophthalmol 120: 701–713.
2. AGIS investigators (2002) The advanced glaucoma intervention study (AGIS): 7. The relationship between control of intraocular pressure and visual field deterioration. Am J Ophthalmol 130: 429–440.
3. Gabelt BT, Kaufman PL (2005) Changes in aqueous humor dynamics with age and glaucoma. Prog Retin Eye Res 24: 612–637.
4. Tan JC, Peters DM, Kaufman PL (2006) Recent developments in understanding the pathophysiology of elevated intraocular pressure. Curr Opin Ophthalmol 17: 168–174.
5. Bustelo XR (2001) Vav protein, adaptors and cell signaling. Oncogene 20: 6372–6381.
6. Schmidt A, Hall A (2002) Guanine nucleotide exchange factors for Rho GTPases: turning on the switch. Genes Dev 16: 1587–1609.
7. Turner M, Billadeau DD (2002) VAV proteins as signal integrators for multi-subunit immune-recognition receptors. Nat Rev Immunol 2: 476–486.
8. Swat W, Fujikawa K (2005) The Vav family: at the crossroads of signaling pathways. Immunol Res 32: 259–265.
9. Riteau B, Barber DF, Long EO (2003) Vav1 phosphorylation is induced byβ2 integrin engagement on natural killer cells upstream of actin cytoskeleton and lipid raft reorganization. J Exp Med 198: 469–474.
10. Gakidis MAM, Cullere X, Olson T, Wilsbacher JL, Zhang B, et al. (2004) Vav GEFs are required for β2 integrin-dependent functions of neutrophils. J Cell Biol 166: 273–282.
11. Holsinger LJ, Graef IA, Swat W, Chi T, Bautista DM, et al. (1998) Defects in actin-cap formation in Vav-deficient mice implicate an actin requirement for lymphocyte signal transduction. Curr Biol 8: 563–572.
12. Cella M, Fujikawa K, Tassi I, Kim S, Latinis K, et al. (2004) Differential requirements for Vav proteins in DAP10- and ITAM-mediated NK cell cytotoxicity. J Exp Med 200: 817–823.
13. Doody GM, Bell SE, Vigorito E, Clayton E, McAdam S, et al. (2001) Signal transduction through Vav-2 participates in humoral immune responses and B cell maturation. Nat Immunol 2: 542–547.
14. Faccio R, Teitelbaum SL, Fujikawa K, Chappel J, Zallone A, et al. (2005) Vav3 regulates osteoclast function and bone mass. Nat Med 11: 284–290.
15. Fujikawa K, Miletic AV, Alt FW, Faccio R, Brown T, et al. (2003) Vav1/2/3-null mice define an essential role for Vav family proteins in lymphocyte development and activation but a differential requirement in MAPK signaling in T and B cells. J Exp Med 198: 1595–1608.
16. Tybulewicz VLJ, Ardouin L, Prisco A, Reynolds LF (2003) Vav1: a key signal transducer downstream of the TCR. Immunol Rev 192: 42–52.
17. Karali A, Russell P, Stefani FH, Tamm ER (2000) Localization of myocilin/trabecular meshwork-inducible glucocorticoid response protein in the human eye. Invest Ophthalmol Vis Sci 41: 729–740.
18. Weinreb RN, Toris CB, Gabelt BT, Lindsey JD, Kaufman PL (2002) Effects of prostaglandins on the aqueous humor outflow pathways. Surv Ophthalmol 47 (suppl. 1): S53–S64.
19. Neufeld AH (1979) Experimental studies on the mechanism of action of timolol. Surv Ophthalmol 23: 363–370.
20. Pfeiffer N (1997) Dorzolamide: Development and clinical application of a topical carbonic anhydrase inhibitor. Surv Ophthalmol 42: 137–151.
21. Tanihara H, Inatani M, Honjo M, Tokushige H, Azuma J, et al. (2008) Intraocular pressure-lowering effects and safety of topical administration of a selective ROCK inhibitor, SNJ-1656, in healthy volunteers. Arch Ophthalmol 126: 309–315.
22. Rao PV, Peterson YK, Inoue T, Casey PJ (2008) Effects of pharmacologic inhibition of protein geranylgeranyltransferase type I on aqueous humor outflow through the trabecular meshwork. Invest Ophthalmol Vis Sci 49: 2464–2471.
23. Honjo M, Tanihara H, Inatani M, Kido N, Sawamura T, et al. (2001) Effects of Rho-associated protein kinase inhibitor, Y-27632, on intraocular pressure and outflow facility. Invest Ophthalmol Vis Sci 42: 137–144.
24. Pang IH, Clark AF (2007) Rodent models for glaucoma retinopathy and optic neuropathy. J Glaucoma 16: 483–505.
25. Aihara M, Lindsey JD, Weinreb RN (2003) Aqueous humor dynamics in mice. Invest Ophthalmol Vis Sci 44: 5168–5173.
26. Chang B, Smith RS, Hawes NL, Anderson MG, Zabaleta A, et al. (1999) Interacting loci cause severe iris atrophy and glaucoma in DBA/2J mice. Nat Genet 21: 405–409.